ALKALI-ACTIVATION OF RECYCLED CONSTRUCTION AND DEMOLITION WASTE AGGREGATE WITH NO ADDED BINDER

Bassani[1]*, M., Tefa[1], L., Russo, A.[1], Palmero[2], P.

(1) Department of Environment, Land and Infrastructures Engineering, Politecnico di Torino, Torino, Italy
(2) Department of Applied Science and Technology, Politecnico di Torino, Torino, Italy

Marco Bassani (* = *corresponding author*)
Phone: +39 011 090 5635, e-mail: marco.bassani@polito.it

Luca Tefa
e-mail: luca.tefa@polito.it

Antonio Russo
e-mail: s220913@studenti.polito.it

Paola Palmero
e-mail: paola.palmero@polito.it

ABSTRACT

The alkaline-activation of aluminosilicate compounds present in fine particles of unselected construction and demolition waste (UCDW) aggregates is investigated here. The aim is to stabilize UCDW aggregates by adding an alkali-activating solution (AAS) composed of sodium hydroxide and sodium silicate and then assess their potential employment in base/subbase road pavement layers. Contrary to the practice in other studies, no industrial-waste by-products (i.e., fly ash, slag precursor) or other components containing silica-aluminates were added to the material. Workability, strength, and stiffness values were evaluated at laboratory temperature (around 25°C) for 7, 28 and 60 days. The resulting mixtures were compared with those containing pure water and a diluted AAS (50% of pure AAS and 50% of water). The resilient modulus of UCDW aggregates compacted with pure AAS was considerably higher than those containing both diluted AAS and water only. Similar conclusions were drawn for the unconfined compressive strength and indirect tensile strength parameters, which for UCDW with pure AAS were comparable to those for ordinary cement stabilized granular materials. These results demonstrate the potential offered by the alkali-activation of aluminosilicate compounds present in fine particles of UCDW. The microstructural observation, carried out by Field Emission Scanning Electron Microscopy, coupled with an elemental analysis performed by Energy Dispersive Spectroscopy, supported the successful alkali-activation of UCDW fines.

KEYWORDS:

Unselected construction and demolition waste aggregate; micro-demolition; alkali-activation; stabilization; recycling; subbase pavement layer.

1. INTRODUCTION

The sustainability of construction activity currently represents the most important challenge in the field of civil engineering. One effective way to pursue sustainability is to use low-impact materials instead of natural aggregates and ordinary binders. In the last decade, the employment of construction and demolition waste (CDW) as alternative aggregates, and the use of alkali-activated binders (AAB) in place of ordinary Portland cement in the civil construction industry have shown great potential. CDW and AAB imply low-energy consumption and low-costs, and their use offers many other environmental benefits particularly in the sphere of resource exploitation and landfill operations.

In 2015, the EU countries alone produced about 821 million tonnes of waste resulting from the construction and demolition of civil works and infrastructures [1]. At a national level, Italy produces about 50 million tonnes of CDW per year [1]. The large-scale reuse of this waste would be environmentally beneficial and would lead to a reduction in the demand for virgin natural materials. In addition, the management of CDW as a resource would lead to a reduction in landfill operations, in line with current EU environmental policies [2].

CDW aggregate consists of a mix of natural/excavated soil (NA/ES), recycled concrete (CC), bituminous mixtures reclaimed from bituminous pavements (RA), and bricks and tiles (BT). Currently, the waste is converted at milling plants into two main forms: selected recycled CDW aggregates separated into the previously mentioned components (CC, RA, BT, NA/ES), or the unselected form in which all components are mixed together (referred to here as unseparated CDW – UCDW).

Recycled CDW aggregate was introduced as a road construction material more than twenty years ago, and has been widely used since in non-structural applications. Following numerous successful case studies on low-traffic volume roads [3], there have been attempts recently to increase and broaden its use. For example, selected recycled CDW has been introduced into a number of structural materials [4], while the unselected form has mainly been used in unbound pavement layers, subgrades, and fills [5, 6, 7, 8]. More recently, significant research has been carried out to test and improve the performance of both UCDW and CDW aggregates as stabilizing agents when used together with ordinary or alternative binders [9, 10, 11, 12, 13].

Alkali-activation has become a common technique used in the production of binders from both precursors (normally aluminosilicate powders) and activators such as strong alkaline solutions (which are normally based on sodium silicate and sodium hydroxide), in order to provide granular materials with strength, stiffness, and durability [14]. The process implies a chemical reaction between aluminosilicate materials and alkali metal silicates, under strong alkaline conditions. The mechanism involves the dissolution of *Al* and *Si* in the alkali medium, the transportation of dissolved species and finally polycondensation, during which the silica (SiO_4) and alumina (AlO_4) tetrahedra organize themselves into a continuous three-dimensional structure [15].

Alkali-activated materials, also referred to as *geopolymers*, are considered a sustainable alternative to ordinary Portland cement (OPC) mainly because the latter is one of the main sources of CO_2 emissions on a global

scale accounting for circa 5% of the total volume (of emissions) [16]. According to Worrell et al. [17], the production of 1 tonne of OPC releases 0.22 tonnes of carbon into the environment, corresponding to 0.689 - 0.822 tonnes of carbon dioxide-equivalent (CO_2-e) [16, 18, 19]. There is a reduction of between 40 to 80% in CO_2-e values for alkali-activated concrete when compared to OPC [20, 21, 22, 23]. However, a recent study by Turner and Collins [24] showed a much lower reduction than in earlier studies: they found that the CO_2 footprint of geopolymer concrete was only 9% less than comparable concrete containing 100% OPC. It must be mentioned that the CO_2-e estimates relating to geopolymer production depend on several factors such as the source of raw materials, the concentration and quantity of the alkaline activators, the manufacturing process, the energy sources, and the transportation distances, etc. These factors may help to explain the different values of CO_2-e determined in the previously mentioned works.

Sodium silicate has been used in construction materials for more than a century. Originally, it was used to solidify soils as per the injection method, while in the middle of the 20th century it was used as a soil stabilizer [25]. The mixture of sodium silicate and sodium or potassium hydroxide has more recently been used to promote the alkali-activation process in granular materials. Although various aluminosilicate industrial by-products have been used in alkali-activation (*i.e.*, fly ash, granulated blast furnace slag, red mud, etc.), the alkali-activation of CDW is still a challenge and a rather limited number of studies have been carried out so far. In fact, some studies have proved that powders obtained from some CDW components (mainly recycled concrete, and bricks and tiles) demonstrate significant alkali-activation potential [26, 27, 28, 29, 30]. However, in all these works, CDW was separated into components and the single fractions were tested in the geopolymer process.

Jha and Tuladhar [31] showed an almost linear increase in the compressive strength of CDW-based geopolymers by increasing the curing time (carried out at 40°C) from 5 to 15 days. Similarly, Pathak et al. [28] showed a continuous increase in the mechanical strength of brick waste-derived geopolymers, by increasing the curing time (at 60°C) from 7 to 28 days. Zedan et al. [30] showed a similar trend for alkali-activated ground granulated blast furnace slag, mixed with 10% of different waste powders (ceramic, red clay brick, and concrete) when cured from 1 to 56 days at room temperature. In contrast, Komnitsas et al. [29] investigated the compressive strength of concrete-, brick- and tile-waste geopolymers, after 7 and 28 days of curing, carried out at 80°C or 90°C. No further increase in strength was observed during curing, a finding which can probably be attributable to the high-temperature curing conditions.

In this research, the authors investigated the behaviour of unselected CDW aggregate (UCDW) mixtures when subjected to alkali-activation in order to evaluate their potential employment in the base and subbase layers of road pavements. To meet this objective, a preliminary X-Ray Diffraction (XRD) analysis was carried out on fines passing at 63 μm to evaluate the presence of aluminosilicate components that, potentially, could be geopolymerized. No other components, such as industrial-waste by-products (i.e., fly ash, slag precursor) or

materials containing silica-aluminates were added to the material, unlike in the previously mentioned research studies.

Two UCDW samples of different size distributions were divided into size classes, and then mixed to follow a reference grading curve. Cylindrical samples of UCDW aggregates with alkali-activating solution (AAS) containing sodium silicate (Na_2SiO_3) and sodium hydroxide (NaOH) were compacted at the Gyratory Shear Compactor (GSC) and then cured at a laboratory temperature of 25°C. The samples were then tested to evaluate their unconfined compression strength (UCS), indirect tensile strength (ITS), and resilient modulus (RM) after 7, 28 and 60 days. In the investigation, a pilot study was also carried out to check in advance if UCDW aggregates samples were potentially sensitive to alkali-activation. Finally, the microstructures and the morphology after alkali-activation and curing were examined through the Field Emission Scanning Electron Microscopy (FESEM) and Energy Dispersive Spectroscopy (EDS) analyses.

2. MATERIALS AND METHODS

2.1 UCDW aggregates properties

Both samples of UCDW recycled aggregates were obtained from a plant in the Turin area (Northwest of Italy), which mainly treats waste materials from the micro-demolition of buildings and road pavements. The finest material was available in the 0-8 mm fraction, while the coarsest was available in the 0-25 mm fraction. Figure 1 provides their grading distributions, as well as the percentage distribution of subcomponents (particles of concrete, asphalt, brick and tiles, aggregates and excavated soils). The particle density values of two different sample grains (γ_g) were estimated according to EN 1097-6 [32], and were equal to 2635 kg/m^3 for UCDW 0-25, and to 2682 kg/m^3 for UCDW 0-8.

The UCDW aggregate materials were first divided into 25, 22.4, 12.5, 8, 4, 2, 0.4, and 0.063 mm size classes (in terms of sieve openings), and then recombined to follow the reference grading curve obtained as the average of the two grading limits of the Italian technical specifications [33]. The design curve shows 100% passing at 25 mm, 95% at 20 mm, 85.6% at 12.5 mm, 67.5% at 8 mm, 50% at 4 mm, 37.5% at 2 mm, 22.5% at 0.4 mm, 11.9% at 0.125 mm, and 9.5% at 0.063 mm. In the investigation, all samples were prepared with this grading curve, and a γ_g of 2664 kg/m^3 was determined for the recombined UCDW aggregate following the design curve plotted in Figure 1. The fraction passing at 0.063 mm, and corresponding to 9.5% of the UCDW sieved material, is supposed to be the most reactive under alkaline conditions. Several authors [29, 34, 35, 36, 37] have, in fact, demonstrated that a decrease in raw material particle size leads to an increase in the mechanical properties of the alkali-activated materials. The finer the material, the shorter the time required for dissolution and completion of the geo-polymerization reactions. This results in stronger bonding and hence increased strength of the final products.

The material components of the UCDW aggregates collected were evaluated on the 10-14 mm size fraction by means of visual inspection, separating the different components (NA/ES, RC, RA, BT). The composition percentage was obtained by dividing the mass of each component by the total mass of the investigated sample (around 20 kg). The results revealed that the UCDW material is characterized by a significant quantity of RA (29%), a finding which contrasts with the data by Agrela et al. [38] and Jiménez et al. [3] who reported RA contents of 4% and 9% respectively. Lower quantities of BT are observed compared to the values recorded by Cerni and Colagrande [39], 30%, and Jiménez et al. [3], 21%. The mass percentages of RC (19%) and NA/ES (41%) are consistent with those in literature.

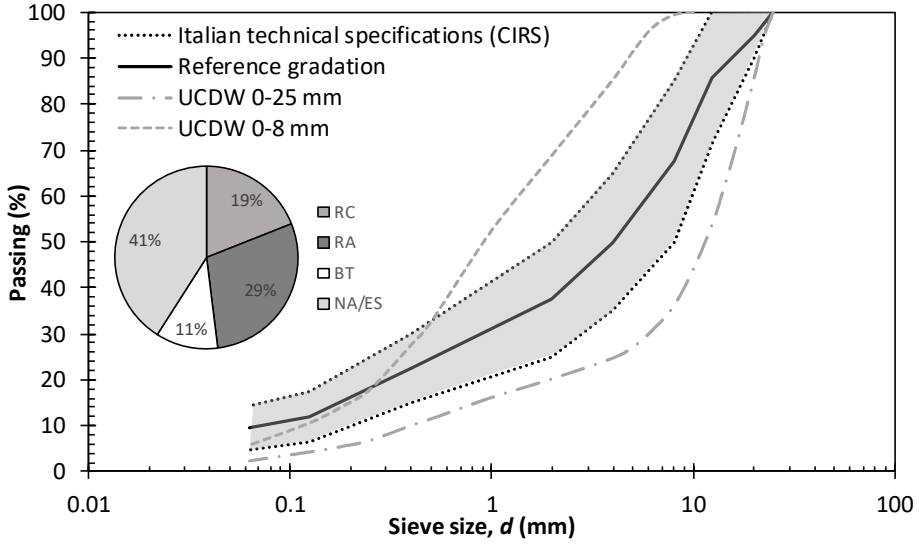

Figure 1. Grain size distribution of the two sources of UCDW aggregates, the design gradation obtained from Italian technical specifications, and composition of subcomponents (RC = recycled concrete, RA = recycled asphalt, BT = brick and tiles, NA/ES = natural aggregates and excavated soils)

2.2 Chemical and phase composition

The fines passing at the 0.063 mm sieve were used to form a small sample for X-Ray Fluorescence (XRF, Rigaku ZSX 100E) and X-Ray Diffraction (XRD, Philips PW 1710) analyses which served to determine the chemical composition of the sample, and the presence of silica and silica-aluminate phases which could undergo alkali activation phenomena. Indeed, according to literature [29], the hypothesis is that the finest fraction of the mineral UCDW powder could undergo alkaline activation. Due to a greater surface area, geopolymerisation reactions proceed much faster than is the case with larger particles, resulting in a more effective stabilization [34].

XRF results, collected in Table 1, show that the material is predominantly composed of silicon (46.10%), calcium (16.40%), aluminium (13.20%) and iron (8.52%) oxides, in addition to non-negligible amounts of alkaline and alkaline-earth oxides, such as MgO (7.62%) and K_2O (2.33%), and smaller amounts of transition metal oxides.

The diffraction pattern depicted in Figure 2 shows the presence of Quartz (SiO_2) and Calcite ($CaCO_3$) in addition to other silicates (Lizardite ($Mg_3Si_2O_5(OH)_4$), Thaumasite ($Ca(SO_4)[Si(OH)_6](CO_3)\cdot 12(H_2O)$) and aluminosilicates (Albite ($NaAlSi_3O_8$), Clinochlore ($(Mg,Fe^{+2})_5Al(Si_3Al)O_{10}(OH)_8$), Wavellite ($Al_3(PO_4)_2(OH,F)_3\cdot 5H_2O$), and Muscovite ($KAl_2(Si_3Al)O_{10}(OH,F)_2$). Together with Quartz, Albite phase is commonly present in bricks, ceramics and concrete and related waste [29, 40, 41]. In general, all the identified phases are typically present in the West Alpine region (specifically Albite, Lizardite, and Clinochlore).

This confirms that the UCDW materials used in the investigation come from aggregates, soils, rocks or alluvial deposits in the Alpine region. In addition, this analysis confirms the presence of aluminosilicate compounds in the powder, as expected following the XRF results, suggesting that the finest fraction of the raw material tends to be reactive in an alkaline environment.

However, it should be pointed out that the extent of the dissolution of aluminosilicate compounds in an alkaline medium depends on the crystallinity of the compounds [42, 43]. In the present case, since the raw material is made up of highly-crystalline mineral phases, only a partial dissolution of *Al* and *Si* species is expected [44]. Therefore, the reactivity of the raw powder was tested by the addition of alkaline solutions at increasingly higher concentration levels, as reported later.

Table 1. Chemical composition of UCDW sieved powder (d < 63 μm) as determined by XRF analysis

Chemical compounds	(%)
SiO_2	46.10
CaO	16.40
Al_2O_3	13.20
Fe_2O_3	8.52
MgO	7.62
SO_3	4.02
K_2O	2.33
TiO_2	0.84
P_2O_5	0.23
MnO	0.22
Cr_2O_3	0.13
NiO	0.09
SrO	0.09
ZnO	0.07
ZrO_2	0.05
CuO	0.03
Rb_2O	0.02

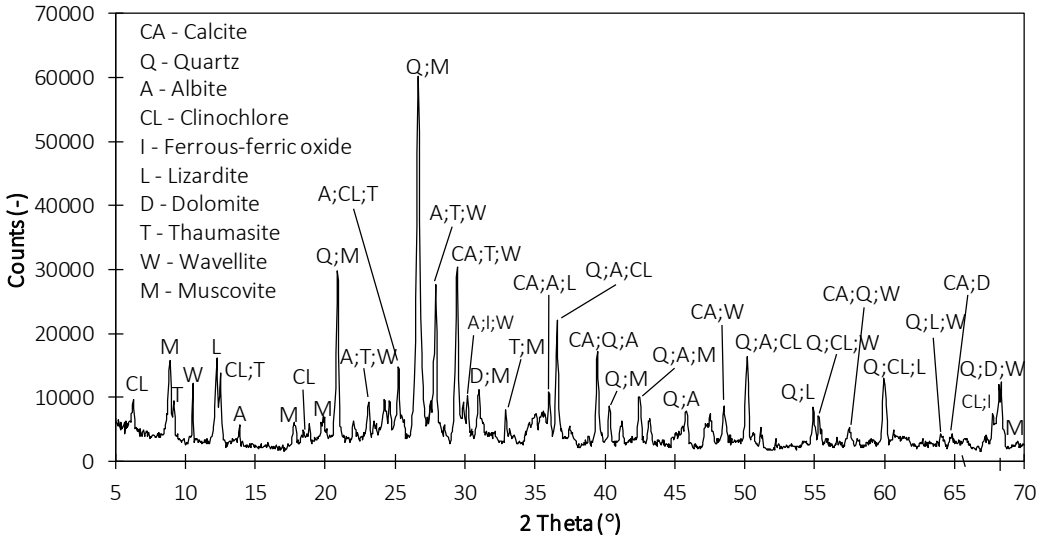

Figure 2. XRD pattern of sieved UCDW powder (d < 63 μm)

2.3 Alkali-activating solution

The alkali-activating solution (AAS) includes sodium hydroxide and sodium silicate. Sodium silicate (Na_2SiO_3) was supplied in liquid form, and was characterized by a modulus (*i.e.*, the SiO_2/Na_2O molar ratio) of 3.4. Sodium hydroxide (NaOH) was supplied in solid form (flakes). The AAS was prepared in two stages: in the first, NaOH flakes were dissolved in distilled water to form an aqueous solution at 50% by weight, with a concentration of 25M; in the second, AAS was produced by mixing NaOH and Na_2SiO_3 solutions in a 1:4 mass ratio.

The AAS was used in both a pure and diluted form with 50% of distilled water. Pure distilled water was also used for comparison purposes. Thus, three solutions labelled as AAS_0% (distilled water), AAS_50% (AAS diluted to 50%) and AAS_100% (AAS without dilution) were employed. A further diluted solution (with 25% of distilled water, AAS_75%) was prepared exclusively for the preliminary pilot study (Section 2.5). The proportion of the components in AAS_50% and AAS_100% are given in Figure 3, from which the final concentration of NaOH (1.5M and 4M, respectively) can be calculated.

Previous studies underlined the pivotal role of the concentration of NaOH when it comes to the ability of CDW components to undergo alkali-activation. Allahverdi and Kani [26] showed a continuous increase in the mechanical strength of bricks and concrete waste in line with an increase in Na_2O content. Other works [31, 41] showed optimal strength values at specific NaOH concentrations. According to these studies, a low NaOH molarity does not provide the system with sufficient alkalinity to undergo geopolymerization reactions. Conversely, a too-high NaOH concentration may result in unreacted alkali, which slows down the geopolymer synthesis process, and consequently solidification and mechanical strength development [43, 45]. In particular, Tchakoute Kouamo et al. [45] advocated an optimal Al_2O_3/Na_2O molar ratio of 0.13 for fused volcanic ash-based geopolymers to achieve the highest geopolymer conversion and compressive strength values. In addition, excess

unreacted sodium hydroxide/oxide may be prone to carbonation and result in the formation of brittle and soluble phases such as Pirssonite, $Na_2Ca(CO_3)_2{\cdot}2H_2O$ [29].

The three solutions were characterized by different densities, 1.00, 1.18, and 1.45 g/cm^3 for AAS_0%, AAS_50% and AAS_100% respectively. In addition, a remarkable increase in viscosity when moving from the less to the more concentrated solution was observed.

Measurements of static viscosity carried out by Yang et al. [46] on a sodium silicate solution having the same modulus and concentration as the silicate used in this work reported a value of 0.0703 Pa s at 25°C (in their experiment, the modulus was controlled by the addition of sodium hydroxide). As a result, the AAS_100% used in this investigation was approximately 79 times higher than for distilled water (whose static viscosity at the same temperature is $0.89{\cdot}10^{-3}$ Pa s). The effects of density, viscosity, and concentration of the AAS on the physical and mechanical properties of the alkali-activated UCDW were considered and will be discussed at a later stage.

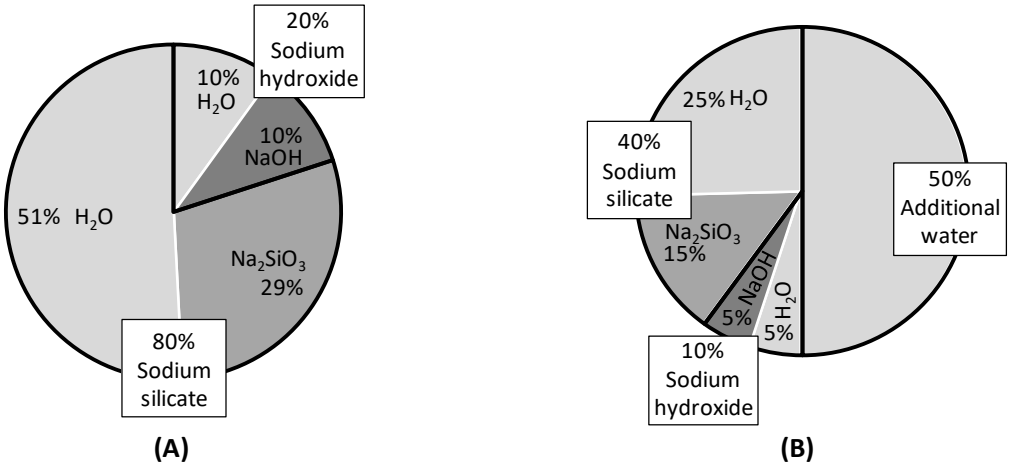

Figure 3. Proportion of components of AAS_100% (A) and AAS_50% (B) with respect to the liquid phase.

2.4 Preliminary compaction study

A preliminary compaction study as per the Proctor method [47] was carried out to estimate the reference optimal AAS content values to reach the best compaction of AAS-UCDW mixtures. Figure 4A shows the evolution of the dry density (γ_d) of AAS-UCDW mixtures as a function of the AAS content (w_{AAS}), an analysis of which identifies the optimal values of AAS which make it possible to reach the maximum γ_d. In the analysis, γ_d was estimated by starting from the wet density of specimens (γ_{wet}), considering w_{AAS} as the liquid content of a three-phase system of an AAS-UCDW mixture:

$$\gamma_d = \frac{\gamma_{wet}}{\left(\frac{w_{AAS}}{100}+1\right)} \quad (1)$$

Figure 4B shows γ_d as a function of the nominal water content (w_w) included in each AAS whose values can be derived from their compositional data reported in Section 2.3. The optimal water content ($w_{w,opt}$) of the three AAS-UCDW mixtures was found to be around 8.6% for all the AAS concentration values.

Furthermore, Figure 4B shows that the maximum dry density of materials ($\gamma_{d,max}$) is influenced by the AAS properties. In the case of materials treated with water only (AAS_0%) it was equal to 2027 kg/m^3, it increased to 2081 kg/m^3 with AAS_50%, and decreases to 1983 kg/m^3 with AAS_100%. Differences in density are attributable to the role played by the higher viscosity of AAS with respect to water. In fact, a more viscous liquid phase in the material increases the internal shear resistance and contrasts the compaction effort, thus leading to a less dense granular structure.

In this investigation, the experimental design was set assuming three moisture contents for all the AAS-UCDW mixtures corresponding to the $w_{w,opt}$ of 8.6%, and the two variations of ±2% around it ($w_{w,opt}$ - 2%, and $w_{w,opt}$ + 2%). Table 2 synthetizes the evaluation of volumetric parameters for the design AAS-UCDW mixtures on the basis of the compaction parameters resulting from the Proctor study.

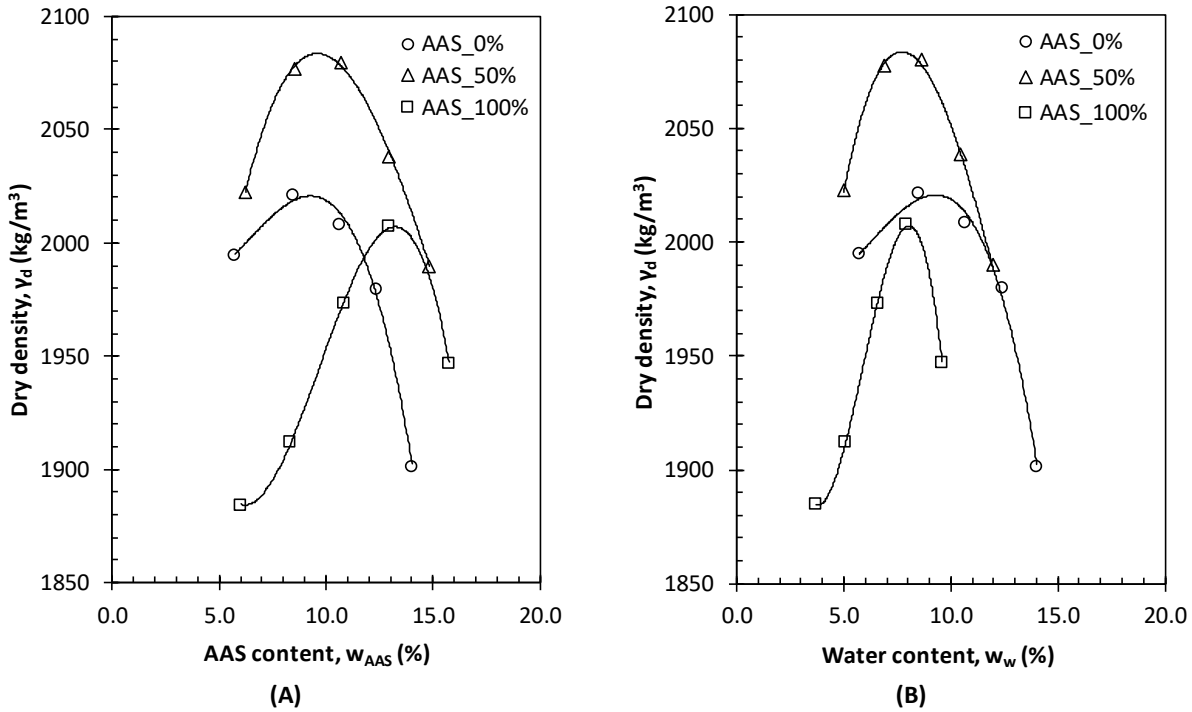

Figure 4. Synthesis of compaction study on UCDW aggregates with different concentrations of AAS. Dry density as a function of AAS content (A) and water content (B)

Table 2. Expected values of saturation in the design AAS-UCDW mixtures

Designation	Water content (w_w) %	AAS type	AAS content (w_{AAS}) %	Wet density[1] (γ_{wet}) kg/m^3	Dry density[2] (γ_d) kg/m^3	Void ratio (e) (-)	Degree of saturation (S) %
$w_{w,opt}$ - 2%	6.6%	AAS_0%	6.6%	2136	2004	0.33	53%
		AAS_50%	8.2%	2244	2074	0.28	65%
		AAS_100%	10.9%	2189	1975	0.35	57%
$w_{w,opt}$	8.6%	AAS_0%	8.6%	2193	2019	0.32	72%
		AAS_50%	10.7%	2301	2078	0.28	86%
		AAS_100%	14.1%	2283	2000	0.33	78%
$w_{w,opt}$ + 2%	10.6%	AAS_0%	10.6%	2227	2014	0.32	87%
		AAS_50%	13.2%	2303	2035	0.31	96%
		AAS_100%	17.4%	2139	1822	0.46	69%

[1] Wet density γ_{wet} derives from the cubic relationship interpolating the measured points during Proctor test.
[2] Dry density is estimated from γ_{wet} as per eq. 1.

In this analysis, the degree of saturation (S) was evaluated to assess whether or not the designed AAS contents would saturate the UCDW granular structure. In the table, S was estimated according to the following equation:

$$S = \frac{w_{AAS} \cdot \gamma_g}{\gamma_{AAS} \cdot e} \quad (2)$$

where γ_g indicates the particle density of the UCDW (2664 kg/m^3), γ_{AAS} the density of AAS (Section 2.3), and e the void index (estimated as γ_g / γ_d).

The values of S in Table 2 affirm that the design AAS-UCDW mixtures would not reach saturation in compaction conditions akin to those of the Proctor one. However, the mixtures presenting higher values of S would be more prone to saturation in the case of a smaller void ratio in the granular matrix. It is worth noting that this would reduce the effectiveness of the compaction effort. It can thus be said that the volumetric data in Table 2 confirm the suitability of design AAS-UCDW mixtures.

2.5 Preliminary pilot study

The experimental investigation was preceded by a pilot study which assessed the mechanical enhancements produced by the addition of AAS to UCDW aggregates. The UCS test after 7 days of curing was carried out on three cylindrical samples of 100 mm in diameter and 200 mm in height prepared at the Gyratory Shear Compactor (GSC). The three samples were mixed with AAS at four different concentrations, (AAS_0%, AAS_50%, AAS_75% and AAS_100%). In accordance with the results previously obtained, the same optimal water content of 8.6% was used in the four AAS-UCDW mixtures.

The results reported in Table 3 clearly indicate that an increase in the concentration of AAS produces an exponential increase in compressive strength. With AAS_50%, the UCS increased more than 4 times with respect

to the same water content without AAS. With AAS_75% the UCS increased more than 9 times, and finally with AAS_100% the UCS increased 25 times. Similarly, large increments of secant and tangent moduli were observed when the AAS was added in place of water.

This evidence demonstrated the effectiveness of alkali-activation at room temperature of the fines present in UCDW aggregates. In light of the differences which emerged between the performances of samples prepared in the AAS_50% to AAS_75% range (Table 3) and those prepared in both the AAS_75% to AAS_100%, and AAS_0% to AAS_50% ranges, the rest of the investigation was restricted to the mixtures containing AAS_0%, AAS_50% and AAS_100%, with the first of these used to provide reference data to indicate the magnitude of AAS stabilization.

Table 3. Synthesis of the pilot study test results for samples after 7 days of curing

AAS type	Water content	UCS	Secant modulus	Tangent modulus
	%	MPa	MPa	MPa
AAS_100%	8.60	3.25	720.8	882.1
AAS_75%		1.20	141.5	178.5
AAS_50%		0.56	74.0	87.2
AAS_0%		0.13	13.3	20.8

2.6 Sample preparation

Cylindrical samples of 100 mm in diameter and 200 mm in height were prepared to investigate UCS and RM as per the repeated load triaxial (RLT) test, while cylindrical samples of 100 mm in diameter and 100 mm in height were prepared to investigate the ITS. To reproduce a simulative densification process, all samples were compacted by the GSC.

The experimental design included 9 mixtures (3 AAS concentration values, and 3 water content values), which generated a total of 108 samples (9 mixtures, 3 curing times, and 4 samples). Table 4 provides a summary of the compositions of all test mixtures, with the last two columns reporting the solid (UCDW) and liquid (AAS) mass values in percentage form. Table 5 includes the experimental plan and the investigated variables.

The UCDW aggregates were mixed with a predetermined quantity of AAS (Table 2). AAS-UCDW mixtures were introduced into the GSC mould in four layers of equal thickness (50 mm). The quantity of mixture required to form a sample was previously estimated considering the expected sample volume (1570.8 cm^3) and the maximum dry density estimated through the Proctor study (Section 2.4 and Table 2). Each layer of samples was compacted with 100 gyrations, with the degree of compaction C_n, which indicates the percentage of the volume occupied by solid particles at the generic *n* gyration, being evaluated as follows:

$$C_n = 100 \cdot \frac{\gamma_d \cdot h_f}{\gamma_g \cdot h_n} \tag{3}$$

where γ_d was estimated at the end of the compaction process, h_n is the height of the sample at a generic (n) gyration which is recorded by the acquisition unit of the GSC, and h_f represents the final height of the sample at the end of compaction (after n = 100 gyrations). Since the trend of C_n is linear when plotted as a function of Log(n), a finding supported by a previous study [48], the analysis of compaction was synthetized through four parameters: the self-compaction (C_1), which is the intercept of the compaction curve per n = 1, the workability (k_g) that corresponds to the slope of the curve, the final compaction (C_{100}), and the residual void content in samples (v = 100 - C_{100}).

Table 4. Synthesis of the compositions of all test mixtures

AAS concentration	Water content	Mass of UCDW (%)	Mass of AAS (%)
0%	$w_{w,opt}$ - 2%	93.8	6.2
	$w_{w,opt}$	92.1	7.9
	$w_{w,opt}$ + 2%	90.4	9.6
50%	$w_{w,opt}$ - 2%	92.4	7.6
	$w_{w,opt}$	90.3	9.7
	$w_{w,opt}$ + 2%	88.3	11.7
100%	$w_{w,opt}$ - 2%	90.2	9.8
	$w_{w,opt}$	87.6	12.4
	$w_{w,opt}$ + 2%	85.2	14.8

Table 5. Synthesis of the experimental plan and investigated variables. Measurements in the table refer to the dimensions of cylindrical samples (h = height, d = diameter)

AAS concentration	Days of curing	Water content	200 (h) x 100 (d) mm		100 (h) x 100 (d) mm
			UCS (*)	RLT	ITS
0, 50, and 100%	7, 28, and 60 days	$w_{w,opt}$ - 2%	2	1	2
		$w_{w,opt}$	2	1	2
		$w_{w,opt}$ + 2%	2	1	2

(*) one of two samples employed in the UCS test was previously subjected to RLT, thus a total of two samples were used to obtain two UCS results and one RM result.

During compaction at the GSC, a part of the AAS was lost, so the AAS content variation Δw_{AAS} was estimated through the difference in weight of loose material before and after compaction, and referred to the starting amount of AAS included in the mixture. Table 6 includes the average of Δw_{AAS} referred to the three sets of samples containing different AAS concentration levels. The results indicate that the loss in AAS was proportionate to the amount of AAS originally in the mixture. In the case of $w_{w,opt}$, the degree of variation in AAS content was sensibly higher in the case of AAS_100%. Samples prepared with w_{AAS} higher than 13% (AAS_50% and AAS_100% with $w_{w,opt}$ + 2%) showed an AAS content variation value of -1.2%. During compaction, the operator noticed that these samples lost a small volume of the liquid above the testing head.

Following compaction, the samples were placed in a plastic mould for protection and storage, and wrapped in cellophane film to prevent any further moisture loss. The samples were cured at room temperature (around 25°C) in a chamber at a relative humidity which was maintained constantly over 90% (sensor range

0÷100% and accuracy of ±3%). After curing and before conducting mechanical tests, they were weighed to assess the moisture variation $\Delta w_{w,cur}$., under the hypothesis that at this stage only the water content could change in the samples. The results of $\Delta w_{w,cur}$ for the full set of samples were between -0.1% and 0% after 7 days, between 0.2% and 0.1% after 28 days, and between -0.2% and 0.3% after 60 days, thus indicating the negligible variation in water content and the effective isolation of samples in the curing environment.

Table 6. Average AAS content variation during compaction at the GSC, Δw_{AAS} (negative values indicate a reduction in AAS content)

AAS type	AAS content variation, Δw_{AAS} (%)		
	$w_{w,opt}$ - 2%	$w_{w,opt}$	$w_{w,opt}$ + 2%
AAS_0%	0.0	-0.1	-0.8
AAS_50%	0.0	-0.2	-1.2
AAS_100%	-0.2	-0.8	-1.2

2.7 Testing protocol

The testing program included the evaluation of ITS, the UCS, and the RM. ITS and UCS tests were carried out at a constant rate of deformation which was set at 0.50 mm/min. Load and displacement data were recorded by a loading cell and a LVDT respectively, and data were sampled at a frequency of 5 Hz.

Technical specifications from national standards mainly refer to ITS and UCS in assessing the quality of stabilized pavement materials. The Italian technical specification of the Ministry of Infrastructures and Transportation [33] indicates a minimum of 0.25 MPa for ITS after 7 days of curing, and a value in the range from 2.5 to 4.5 MPa for UCS.

The RM test is considered the most representative stiffness parameter for granular materials in pavement layers, since it is evaluated under simulative stress-strain conditions and loading time duration. In this investigation, RM was estimated according to the AASHTO T 307-99 base/subbase protocol [49].

Following alkali-activation and curing, the microstructures and morphology of some selected samples were observed by Field Emission Scanning Electron Microscopy (FESEM, ZEISS Supra 40) equipped with an Energy Dispersive Spectroscopy system (Oxford EDS microanalysis). To evaluate the effects of AAS concentration and water content, the procedure was performed on samples prepared with AAS_0% and AAS_50% at the w_{opt}, and on all the samples prepared with AAS_100% (*i.e.*, $w_{w,opt}$ - 2%, $w_{w,opt}$, $w_{w,opt}$ + 2%). All the analyses were performed after 60 days of curing at room temperature. Samples prepared with AAS_100% were also subjected to EDS microanalysis of the binding layer between particles and thus provide confirmation of the geopolymerization of UCDW fines.

3. RESULTS AND DISCUSSION

3.1 Compaction and workability

Figure 5 shows the evolution of the degree of compaction for the samples with an average behaviour of the nine mixtures prepared for this investigation. Each graph includes the compaction curves for mixtures containing AAS_0% (Figure 5A), AAS_50% (Figure 5B), and AAS_100% (Figure 5C), with each curve corresponding to a specific water content. For samples prepared with water only (AAS_0%), an increase in water content results in a rise of the compaction curve mainly due to an increment of C_1 (Figure 5A), while a completely different evolution was observed in the case of mixtures with AAS_50% and AAS_100%.

The AAS_50%-UCDW mixture showed considerable variation in both C_1 (from 68.0% for $w_{w,opt}$, to 63.9% for $w_{w,opt}$ - 2%, and to 56.6% for $w_{w,opt}$ + 2%), and k_g (from 7.5 for $w_{w,opt}$, to 6.1 for $w_{w,opt}$ - 2%, and to 4.1 for $w_{w,opt}$ + 2%). Variations for AAS_100%-UCDW mixtures are larger again. C_1 ranged from 69.7% for $w_{w,opt}$ - 2%, to 61.3% for $w_{w,opt}$, and to 60.2% for $w_{w,opt}$ + 2%, while k_g varied from 7.4 for $w_{w,opt}$, to 2.0 for $w_{w,opt}$ - 2%, and to 0.6 for $w_{w,opt}$ + 2%.

With the aim of achieving a better understanding of the volumetric characteristics of samples at the end of the gyratory compaction process, Table 7 contains the mean, standard deviation, and coefficient of variation (C.V.) for the compaction parameters (C_1, C_{100}, and k_g), residual void content after compaction (v), dry density of samples (γ_d), and degree of saturation (S) for the entire set of 108 samples. The decay in C_1 and k_g which affected the three AAS-UCDW mixtures with the highest AAS concentration can be explained partly by the degree of saturation, and partly by the viscosity of AAS. AAS-UCDW mixtures close to saturation (*i.e.*, mixture with AAS_50% and w_{opt} + 2%; and mixture with AAS_100% and prepared at w_{opt} and w_{opt} + 2%) experienced a slight reduction in their height during compaction.

To interpret data in Table 7, it is worth noting that measurements of γ_d and S are related to unloaded samples. Under loading, higher densities and degrees of saturation are expected due to the compression of the granular matrix by the testing heads. This also explains the loss of AAS exhibited by more saturated samples documented in Table 6.

Furthermore, the fact that the three AAS solutions exhibit different viscosity values explains the difficulties in compaction of mixtures with a large AAS content. In fact, the saturation of samples prepared with AAS_0% and $w_{w,opt}$ + 2% equal to 87.1 ± 1.7%, is sensibly higher than that of the AAS-UCDW mixture prepared with AAS_100% and $w_{w,opt}$ (79.2 ± 1.8%), despite the first set of samples proving to be more workable than the second one. This confirms that the viscosity of more concentrated solutions contrasted the packing action of GSC testing heads.

C.V. values included in Table 7 indicate that samples of the same mixture were very similar to each other. The C.V. of γ_d is always lower than 0.8%, which illustrates the very small variation in packing conditions between

samples of the same mixture. The sole exception was for AAS_100% with $w_{w,opt}$ + 2% which exhibited a C.V. equal to 2.2%. Finally, k_g of the mixtures with w_{AAS} higher than 13% exhibited the largest values of C.V.

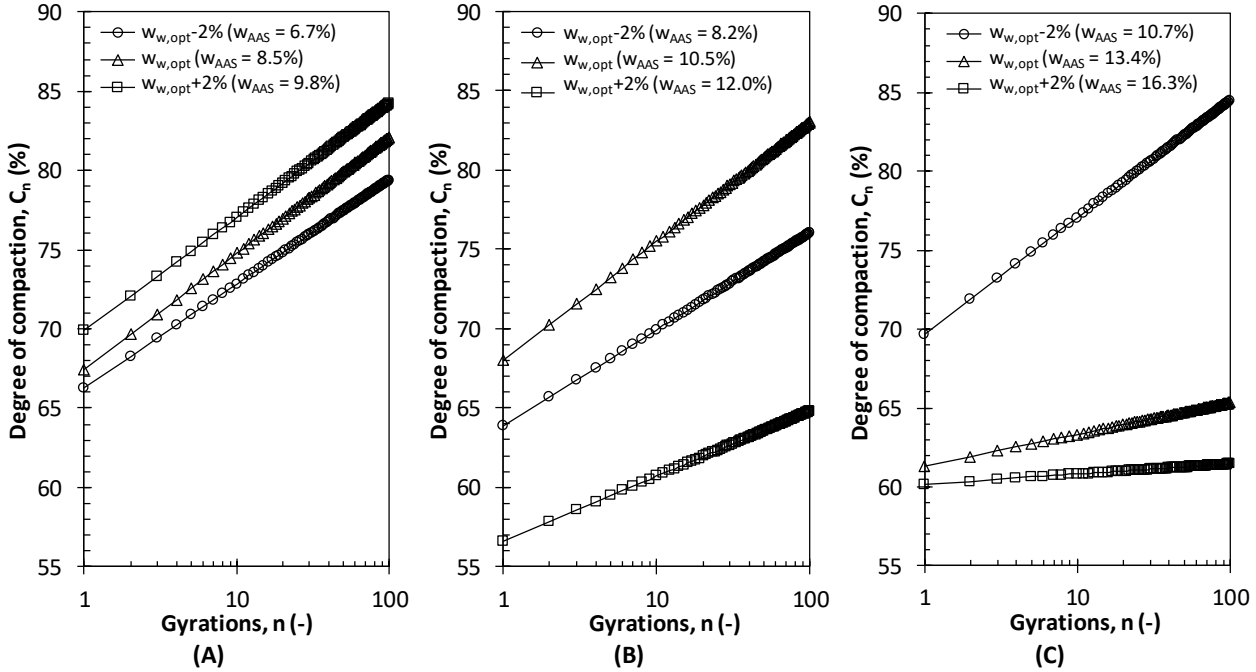

Figure 5. Compaction curves for average samples prepared with AAS_0% (A), AAS_50% (B), and AAS_100% (C) for three AAS contents in the granular matrix

Table 7. Synthesis of the average self-compaction (C_1), workability (k_g), final dry density (γ_d), final compaction (C_{100}), void content (v), and degrees of saturation (S) of investigated samples (st.dev. = standard deviation, C.V. = coefficient of variation in %)

AAS concentration		AAS_0%			AAS_50%			AAS_100%		
		mean	st.dev.	C.V. (%)	mean	st.dev.	C.V. (%)	mean	st.dev.	C.V. (%)
C_1 (%)	$w_{w,opt}$ - 2%	66.3	0.7	1.0	63.9	5.6	8.7	69.7	0.4	0.6
	$w_{w,opt}$	67.4	1.0	1.5	68.0	1.3	1.9	61.3	4.6	7.5
	$w_{w,opt}$ + 2%	69.9	2.0	2.8	56.6	4.1	7.3	60.2	0.4	0.7
k_g (-)	$w_{w,opt}$ - 2%	6.5	0.2	2.8	6.1	0.4	6.5	7.4	0.4	5.8
	$w_{w,opt}$	7.3	0.2	3.4	7.5	0.4	5.5	2.0	0.4	18.2
	$w_{w,opt}$ + 2%	7.2	0.4	5.7	4.1	1.1	26.7	0.6	0.1	13.9
C_{100} (%)	$w_{w,opt}$ - 2%	79.4	0.9	1.1	76.0	5.0	6.6	84.5	0.9	1.1
	$w_{w,opt}$	82.1	1.3	1.6	83.0	1.9	2.3	65.3	5.2	7.9
	$w_{w,opt}$ + 2%	84.2	1.3	1.6	64.8	5.6	8.6	62.8	4.7	7.5
v (%)	$w_{w,opt}$ - 2%	20.6	0.9	4.4	24.0	5.0	21.0	15.5	0.9	5.8
	$w_{w,opt}$	17.9	1.3	7.2	17.0	1.9	11.4	34.7	5.2	14.9
	$w_{w,opt}$ + 2%	15.8	1.3	8.5	35.2	5.6	15.8	37.2	4.7	12.7
γ_d [kg/m^3]	$w_{w,opt}$ - 2%	2064	6	0.3	2028	17	0.8	2052	11	0.5
	$w_{w,opt}$	2056	9	0.5	2056	8	0.4	2023	12	0.6
	$w_{w,opt}$ + 2%	2049	12	0.6	2044	9	0.5	1971	44	2.2
S (%)	$w_{w,opt}$ - 2%	61.0	1.1	1.8	59.3	2.1	3.5	66.2	1.5	2.3
	$w_{w,opt}$	76.9	1.6	2.0	80.6	1.2	1.4	79.2	1.8	2.3
	$w_{w,opt}$ + 2%	87.1	1.7	1.9	91.3	2.0	2.2	87.8	6.6	7.5

Figure 6 exhibits the evolution of C_1 and k_g for the nine mixtures investigated as a function of the actual AAS content ($w_{AAS,real}$), calculated as the difference between the AAS quantity introduced at the beginning of the mixing phase (reported in Table 2) and the loss measured after compaction (Table 6). Each value is associated with a dispersion bar which indicates the standard deviation (listed in Table 7) of 12 samples of each AAS-UCDW mixture.

The bar between points highlights the presence of peak values for C_1 and k_g associated with all the investigated AAS-UCDW mixtures. Results show that peaks for both variables are reached for an AAS content between 10 and 11%, independently of the AAS concentration. At these values, the AAS_50% at $w_{w,opt}$ and AAS_100% at $w_{w,opt}$ - 2% were the most workable AAS-UCDW mixtures. This evidence will be considered in future investigations aimed at the definition of optimal AAS quantities in UCDW stabilized mixtures as per the GSC test.

In this investigation, the discrepancy between the AAS optimum content values obtained from the Proctor and the GSC tests stems from the different interaction between liquid and solid particles which occurs when the samples are compacted. The GSC testing heads produce a kneading action and a rotation of the mould that implies the movement of the liquid phase in the sample, and leads to a leakage of excess liquid from the mould [50].

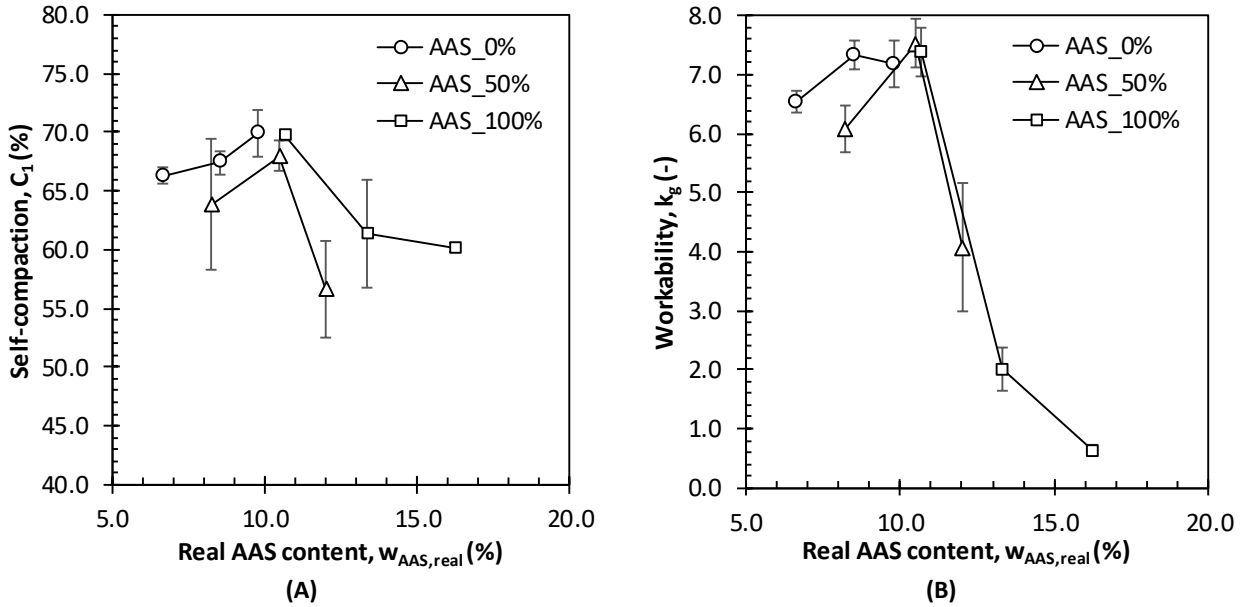

Figure 6. Self-compaction (A) and workability (B) trend in function of the real solution content in the UCDW aggregate

As a result, in the GSC the solid grains tend to get closer and reach a higher dry density than in the corresponding cases investigated as per the Proctor compaction mode, in which the hammer mass impacts on small portions of the sample. In this case, the neutral pressure in the liquid dissipates locally around the volume hit with the compacting mass, so at the end of the compaction process the liquid tends to remain in the sample, thus leaving a greater distance between grains than in GSC samples. This explains why the dry densities in Table

2 are lower than those in Table 7 in all cases where there was a loss of liquid during GSC compaction (*i.e.*, the three mixtures prepared with $w_{w,opt}$ + 2%, and the AAS_100% at $w_{w,opt}$, as evidenced in Table 6).

3.2 Unconfined compression strength

Figure 7 contains a synthesis of the test results and the contribution of different mix-design factors to the UCS of the investigated mixtures. It is worth noting that each single factor considered in the graph produces significant variation in the response variable (UCS).

The effects of alkali-activation were significant only for samples prepared with AAS_100%. In this case, after only 7 days of curing, the UCS ranges from 0.51 MPa (at $w_{w,opt}$ + 2%) to 2.99 MPa (at $w_{w,opt}$ - 2%), with a value of 1.72 MPa for samples prepared at the optimal moisture content (at $w_{w,opt}$). This result highlights the promising performance levels attained by alkali-activated UCDW aggregate mixtures, especially considering the specifications for subbase layer materials. Italian specifications for cement stabilized natural aggregates to be used in subbases require a UCS value in the range 2.5 to 4.5 MPa after 7 days of curing [33].

Table 8 synthetizes the UCS test results reported in literature for several mixtures obtained from natural and recycled aggregates which were stabilized with a variety of ordinary and alternative binders. From an examination of this data, it is worth noting that the values of AAS-UCDW mixtures with $w_{w,opt}$ - 2% after 7 and 28 days of curing are higher than those of Arulrajah et al. [12] on single CDW components with cement kiln dust (CKD), and those reported in Bassani et al. [13] on UCDW mixtures stabilized with OPC and CKD.

After 7 days of curing, the UCS data recorded in this investigation are comparable with those of UCDW aggregates stabilized with 3% of OPC reported by Del Rey et al. [10], and are within the ranges of UCS recorded on cement stabilized natural aggregates. AAS-UCDW mixtures with $w_{w,opt}$ show UCS values of a similar magnitude as UCDW stabilized with OPC and CKD [13], and UCDW stabilized with alkali-activated fly ash [51], although after 28 days, the data in this literature present higher values.

AAS-UCDW mixtures prepared with $w_{w,opt}$ + 2% exhibited UCS test results lower than those obtained for recycled and natural materials stabilized with cement or by-products after 7 and 28 days of curing. In mixtures including $w_{w,opt}$ + 2%, UCS increases significantly only after 60 days of curing reaching values close to 2 MPa. The use of AAS_50% determines a small improvement in UCS: values were approximately twice those of the UCS for AAS_0% samples. More evident is the contribution of AAS_100% that led to UCS values about 10 times higher than those recorded for AAS_0% specimens.

The benefit of using highly concentrated AAS has been evidenced in literature [28, 52, 53]. The pH of the mixture is one of the more influential parameters affecting the mechanical strength of the alkali-activated materials. At high pH values, there is a higher degree of dissolution of aluminosilicates, leading to a greater amount of dissolved silica and alumina species in the sol, to a more interconnected inorganic network at the condensation stage, and finally to enhanced mechanical properties in the hardened samples [54].

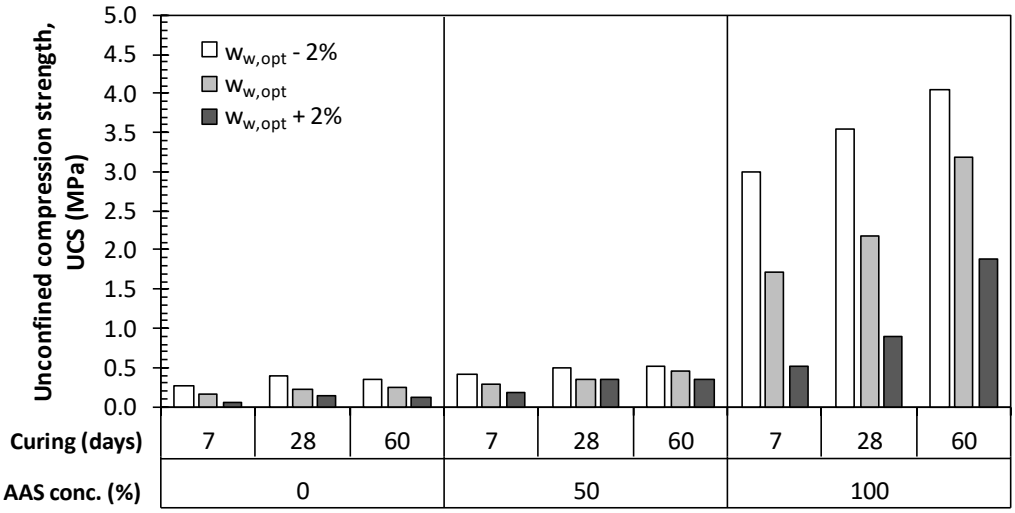

Figure 7. UCS of AAS-UCDW mixtures including three different AAS concentrations (0%, 50% and 100%) after 7, 28 and 60 curing days

Table 8. Synthesis from literature of the UCS values (in MPa) of aggregates (natural and recycled) stabilized with ordinary and alternative binders

Author	Materials	7-day cured	28-day cured
Arulrajah et al. [12]	RA1 + 30% CKD4 (0-12 mm)	2.5	-
	RC2 + 30% CKD4 (0-20 mm)	2.5	-
	RC2 + 30% FA5 (0-20 mm)	0.5	-
	BT3 + 30% CKD4 (0-20 mm)	2.0	-
Bassani et al. [13]	UCDW + 2% OPC6 (0-25 mm)	1.6	2.6
	UCDW + 2% OPC6 (0-8 mm)	1.4	1.8
	UCDW + 10% CKD4 (0-25 mm)	2.3	3.1
	UCDW + 10% CKD4 (0-8 mm)	2.0	3.1
Cristelo et al. [51]	80% UCDW + 20% FA5 alkali-activated	1.6	6.1
	80% natural aggregates + 20 FA5 alkali-activated	1.0	4.5
Del Rey et al. [10]	UCDW + 3% OPC6 (0-40 mm)	2.5 ÷ 3.5	3.1 ÷ 4.2
	UCDW + 3% OPC6 (0-8 mm)	2.6 ÷ 3.4	3.3 ÷ 4.4
Kien et al. [55]	BT3 + 5% OPC6	-	0.8
	RC2 + 5% OPC6	-	1.5
	Natural quarry materials + 5% OPC6 (0-5 mm)	-	1.0
Mohammadinia et al. [56]	BT3 + 2 % OPC6 (0-20 mm)	2.9	3.1
	RC2 + 2 % OPC6 (0-20 mm)	2.8	3.3
	RA1 + 2 % OPC6 (0-20 mm)	3.1	4.2
Biswal et al. [57]	Lateritic soil (GW7) + 3% OPC6	2.5	2.9
	Lateritic soil (SW7) + 3% OPC6	2.8	3.9
Lim and Zollinger [58]	Crushed limestone base material + 4% OPC6 (0-30 mm)	3.2 ÷ 4.3	3.8 ÷ 7.0
Piratheepan et al. [59]	Soil + BFS8 and lime (0-19 mm)	-	3.4
Davis et al. [60]	Weak soil subgrade material + 4 % OPC6 (0-25 mm)	1.2 ÷ 3.0	-

([1]) RA = Recycled Asphalt, ([2]) RC = Recycled Concrete, ([3]) BT = Bricks and Tiles, ([4]) CKD = Cement Kiln Dust, ([5]) FA = Fly Ash, ([6]) OPC = Ordinary Portland Cement, ([7]) according to ASTM D 2487 classification [61], ([8]) BFS = Blast Furnace Slag.

In addition, it is worth mentioning that typical geopolymer products are prepared starting from amorphous or semi-crystalline aluminosilicate raw powders (e.g., calcined clays, fly ash, silica fume and granulated blast furnace slag, etc.) [62, 63, 64, 65] which show high reactivity under alkaline conditions. In contrast, in the material presented here, the starting aluminosilicate raw powders are mineral and highly crystalline (Figure 2), with a considerably lower degree of dissolution [44]. In such conditions, the AAS

concentration is assumed to have even greater importance. This is supported by the results of this investigation, which indicate a clear increment in strength only when the most concentrated solution (AAS_100%) is employed.

It is also important to mention the role of sodium silicate in AAS, in that it can increase the mechanical strength of the alkali-activated materials. In fact, according to Duxson et al. [66] and Pacheco-Torgal et al. [67], sodium silicate can generate soluble silica species (Si-O-) which promote the formation of the geopolymer structure. In addition, sodium silicate provides a strong interface between the non-reacting particles and the gel matrix, thus contributing to overall mechanical strength [68].

Considering the presence of highly-crystalline raw powders in this investigation, it is reasonable to suppose that the mechanical strength value was due to the synergic effects of the solidification of sodium silicate and the alkaline activation of the finest waste fraction. This hypothesis is supported by the fact that strength increases with curing time, suggesting a completion of hydration and geopolymerization reactions during the 28-day curing period. In fact, Figure 7 highlights that curing time is beneficial to the evolution in strength of the investigated materials independently of the quantity or concentration of AAS. This result also suggests that UCS continues to increase after 28 days of curing, so the completion of hydration and geopolymerization reactions at laboratory temperature would be achieved after 28 days. Accordingly, curing at higher temperatures would lead to the asymptotic (long term) UCS value in a shorter time frame [29].

Figure 7 also evidences the negative effects produced by an increased quantity of AAS since, in all cases, UCS decreases when the quantity of AAS (and water) increases. This is more evident in the case of AAS_100% samples: the excessive volume of liquid AAS in the compaction stage reduced the effectiveness of the packing action promoted by the testing heads as evidenced in Section 3.1 (Figure 5C). The embedding of compressed air bubbles within the granular structure is another procedure that could condition the strength of the hardened material, since it can create internal stresses in the void pores. Furthermore, the curing was carried out under wet conditions with samples wrapped in cellophane film to avoid any water loss (see Section 2.6). This induces a decrease in the concentration of -OH in the pore solution and possibly a reduction in the rate of geopolymerization at a subsequent stage, as postulated by Naghizadeh and Ekolu [69]. Thus, in this work, the higher the water content, the lower the geopolymerization rate observed.

3.3 Indirect tensile strength

Tensile strength test results as per the indirect test method are synthetized in Figure 8. The trend in data is similar to that depicted in Figure 7 for UCS. AAS_100%-UCDW mixtures delivered excellent results also in terms of ITS. After 7 days of curing, mixtures prepared at $w_{w,opt}$ and at $w_{w,opt}$ - 2% resulted in values superior to the minimum of 0.250 MPa indicated by Italian technical standards [33] as a requisite for cement stabilized granular materials in subbase layers. AAS_100%-UCDW mixtures exhibited the remarkable value of 0.573 MPa with a real AAS quantity of 8.2% (corresponding to $w_{w,opt}$ - 2%), and 0.267 MPa with 10.5% AAS (corresponding to $w_{w,opt}$).

Similarly to the case of UCS, an excess of liquid determined a reduction in ITS to 0.128 MPa for 12.0% of AAS in the mixture (corresponding to $w_{w,opt}$ + 2%).

The improvement in ITS over time is illustrated in Figure 8. An increase of 24% was observed passing from 7 to 28 days for mixtures including AAS_100%, while +18% was recorded passing from 28 to 60 days of curing. In the long term, this trend leads all the investigated mixtures prepared with AAS_100% over the threshold of 0.250 MPa required by Italian technical specifications for subbase layers at 7 days. Results obtained with the addition of AAS_50% failed to meet the requirements for stabilized subbase materials, with only slight increments in ITS over time. The results obtained here are comparable to those of Kien et al. [55], who found ITS values for BT, RC and a natural quarry material, after 28 days of curing and stabilization with 10% of OPC, equal to 0.35, 0.77 and 0.58 MPa respectively.

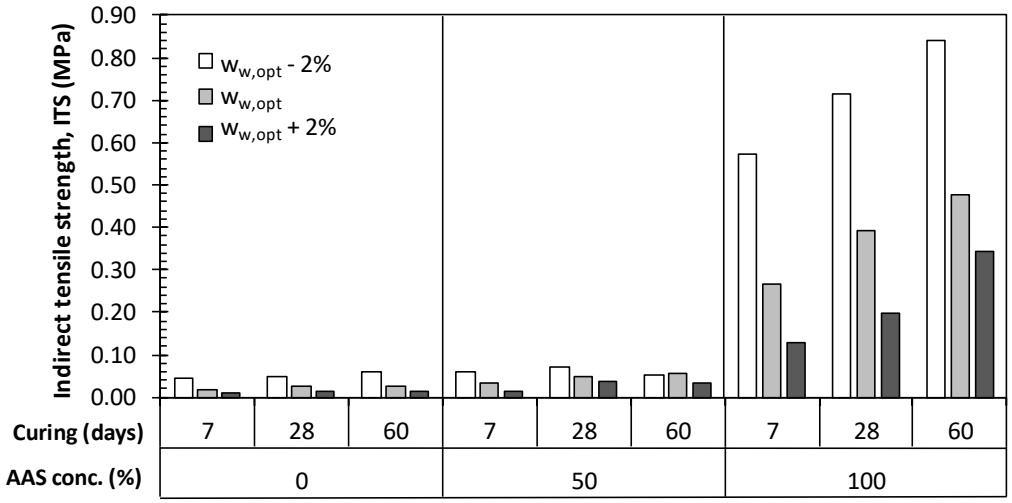

Figure 8. ITS of AAS-UCDW mixtures including three different AAS concentrations (0%, 50% and 100%) after 7, 28 and 60 curing days

3.4 Resilient modulus

The stiffness of AAS-UCDW mixtures as per the RLT test are synthetized as a function of curing time and for the same AAS content (corresponding to w_{opt}) in Figure 9, and as a function of AAS content in Figure 10. The two figures include regression lines for each set of data to interpret the dependency of RM on the first stress invariant θ (*i.e.*, the sum of the three principal stress peaks in the samples during the test, $\theta = \sigma_1 + \sigma_2 + \sigma_3$, also known as "bulk stress").

After 7 days, the AAS_100%-UDCW mixture exhibited the highest RM, while values for the other two mixtures (those containing AAS_0% and AAS_50%) were similar as already observed with UCS and ITS, although slightly higher RM values for the AAS_0%-UCDW were observed (Figure 9A). The RM of UCDW aggregates with AAS_50% and AAS_0% improved at 28 and 60 days with respect to 7 day-cured samples in the region of low θ.

At the first stress condition of the RLT test (θ = 82.8 kPa, σ_1 = 41.4 kPa, $\sigma_{2,3}$ = 20.7 kPa) the RM of AAS_50% passed from 66.7 MPa at 7 days to 127.4 MPa at 28 days. Similarly, for AAS_0% the RM passed from 69.2 MPa at 7 days to 105.7 MPa at 28 days. No significant improvement in RM was recorded at more severe stress conditions.

Conversely, in the case of the AAS_100%-UCDW mixture, the increment in resilient response is evident at the highest stress condition after 60 days of curing (Figure 10). At the last loading sequence (θ = 689.5 kPa, σ_1 = 413.7 kPa, $\sigma_{2,3}$ = 137.9 kPa) the RM increases by 35% passing from 28 to 60 days of curing.

Although affected by variation in test results due to uncontrolled variables in the preparation of samples, the indications from testing suggest that AAS_100% provides the best stress-strain response, while UCDW aggregates with AAS_0% and AAS_50% exhibited similar responses independently of curing time in the range from 7 to 60 days. New internal bonds in the granular matrix due to alkali-activation (in the case of AAS_50%) and hydration processes (potentially for both AAS_50% and AAS_0%) are too weak to provide significant increments over time in RM.

Figure 10A illustrates the RM of samples prepared with AAS at 100% concentration with a variable AAS content after 7 days of curing. It is worth remembering that those samples were characterized by very different void content values (Table 7). Samples prepared with the highest AAS content ($w_{w,opt}$ - 2%) contain on average 15.5% of voids in the solid matrix, those with $w_{w,opt}$ contain 34.7% of voids, and those at $w_{w,opt}$ + 2% a void content of 37.2%. A granular matrix with high void content is normally less stiff than a denser one, so this explains why the sample with the highest AAS content ($w_{w,opt}$ + 2%) exhibited the lowest stiffness initially, while the sample prepared with $w_{w,opt}$ - 2% proved to be the stiffest one. Looking at the graph, the sample containing $w_{w,opt}$ was found to be the stiffest but only at the lowest stress condition of the AASHTO T 307-99 protocol [49].

At the longer curing times of 28 (Figure 10B) and 60 days (Figure 10C), the RM values of mixtures prepared with a higher AAS content increased sensibly with respect to those recorded after only 7 days. In particular, after 60 days the results of the three different samples tend to converge. In this case, time has allowed the development of the alkali-activation process, which was more pronounced in mixtures richer in AAS. In the long term, AAS-UCDW mixtures with a higher AAS content tend to compensate for the initial low RM due to a lack of compaction, with more bonds developing in the granular matrix. This is a promising result for field applications, because local excesses of or deficiencies in AAS in the layer do not alter the homogenous stiffness response to load applications that may occur over time.

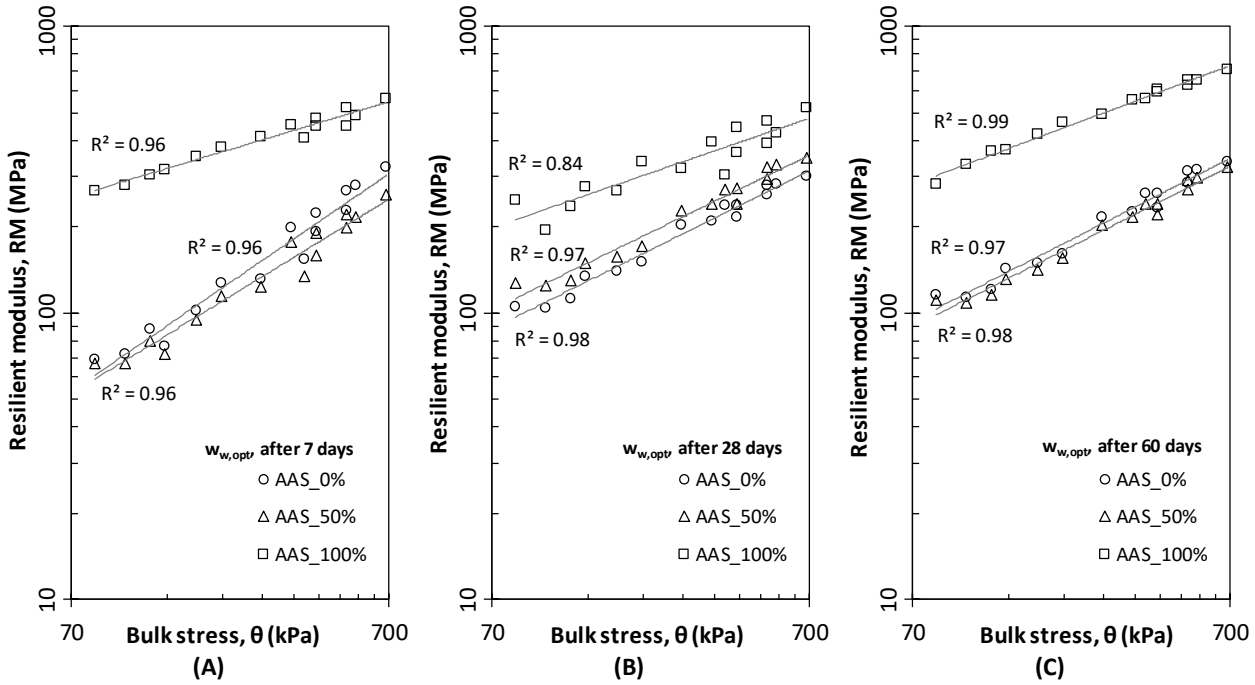

Figure 9. RM of UCDW aggregates mixed with AAS in three different concentrations (0%, 50% and 100%) for specimens compacted with the optimum moisture content ($w_{w,opt}$) after 7 (A), 28 (B) and 60 (C) curing days

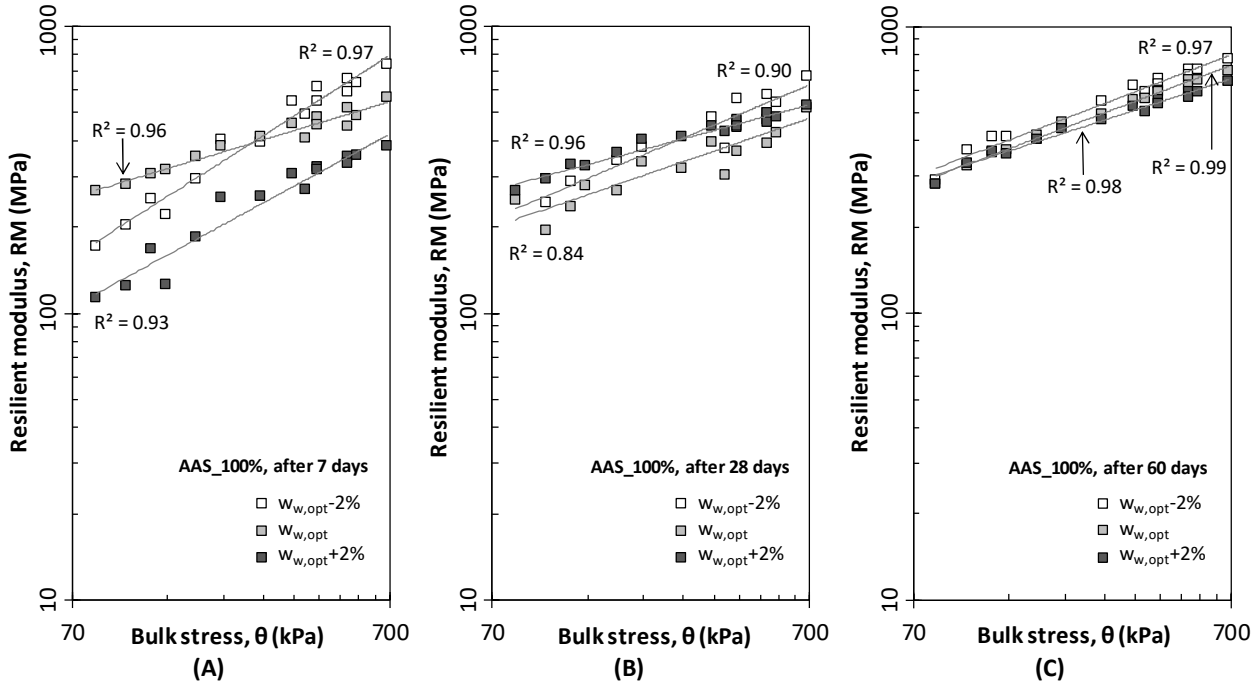

Figure 10. RM of AAS-UCDW mixtures with AAS concentration equal to 100% (AAS_100%) for three different water content ($w_{w,opt}$ – 2%, $w_{w,opt}$, $w_{w,opt}$ + 2%) after 7 (A), 28 (B), and 60 (C) curing days

The results of the fifteen loading sequences of RM testing have been fitted according to the generalized model suggested by the Mechanistic-Empirical Pavement Design Guide [70]:

$$RM = k_1 \cdot p_a \cdot \left(\frac{\theta}{p_a} \right)^{k_2} \cdot \left(\frac{\tau_{oct}}{p_a} + 1 \right)^{k_3} \quad (4)$$

where τ_{oct} is the octahedral shear stress, p_a is the atmospheric pressure, while k_1, k_2, and k_3 are calibration factors of the model which depend on the material properties.

Table 9 contains the synthesis of fitting parameters and the coefficient of determination R^2 of the RM results for each AAS-UCDW mixture. The k_1 parameters, proportional to the stiffness of material, are generally higher after long term curing (28 days or 60 days) than after only 7 days of curing. When UCDW is mixed with water only (AAS_0%), k_1 increases by decreasing the water content, as evidenced in literature [71]. The highest values of k_1 pertain to samples prepared with AAS_100%: values are approximately twice bigger than those of AAS_50%.

k_2 is always positive, indicating that AAS-UCDW mixtures, independently of AAS content and concentration, exhibit a hardening behaviour when the bulk stress increases. This is typical for unbound and stabilized granular materials [72, 73]. Results for AAS_100% indicate lower values than for the other two AAS concentrations. Fluctuations in k_2 water content and AAS concentrations also depend on the value assumed by the other two parameters.

Most of the differences in behaviour between materials occur in the case of k_3. A positive value stands for a shear-hardening behaviour for increment of τ_{oct}, while a negative value reflects a shear-softening behaviour [74]. Results in Table 9 indicate that k_3 is always positive for samples tested after 7 days of curing, while it turns negative in the case of UCDW mixed with AAS_0% and AAS_50% (with the exception of UCDW with AAS_50%). Conversely, a shear-hardening behaviour was evident in AAS_100%-UCDW mixtures, with k_3 values always positive and significantly higher than zero. For this mixture type with various AAS content values, passing from 28 to 60 days, k_1 sees a significant improvement (from 2124÷2970 to 3275÷3537), while the decrease in k_3 (from 0.200÷0.694 to 0.093÷0.160) is compensated by the increase in k_2 (from 0.205÷0.283 to 0.303÷0.377).

For comparison purposes, Table 10 synthetizes the values for the three model parameters of eq. 4 for non-stabilized [73, 75, 76, 77], and stabilized [13, 78, 79] granular materials. If, in the first case, data were estimated from tests carried out immediately after compaction (with the exception of UCDW aggregates investigated after 30 days by Farias et al. [75]), in the second case data all relate to cured samples at 28 days. The most significant difference between stabilized and non-stabilized granular materials is in k_1, which is normally below 1500 for the first material type, and above 1000 for the second. No specific trend is evident in the case of k_2, which varies from 0.01 to 0.98 for non-stabilized materials, and from -0.02 to 1.84 for stabilized ones. Similar conclusions can be drawn for k_3, which is normally negative between -3.44 and -0.09. Exceptions are UCDW after 30 days of curing (1.25), and the A-2-4 stabilized with 3% of Portland cement (between -0.09 and 0.54).

If the *k* factors for UCDW mixtures containing AAS_0% and AAS_50% seem to be similar to data for non-stabilized materials, mixtures including AAS_100% are more similar to stabilized ones for k_1 which ranges between 2124 and 2970, and k_2 ranging between 0.205 and 0.283. Conversely, k_3 is positive between 0.200 and 0.694: this difference confirms the tendency of AAS-stabilized UCDW to exhibit a shear hardening behaviour which is rarely observed in the case of stabilized materials.

Table 9. Results of M-EPDG model fitting (k_1, k_2, and k_3 are model parameters, R^2 is the coefficient of determination)

AAS type	w_w	k_1			k_2			k_3			R^2		
		7 d	28 d	60 d	7 d	28 d	60 d	7 d	28 d	60 d	7 d	28 d	60 d
AAS_0%	$w_{w,opt}$ - 2%	1027	1809	1822	0.607	0.535	0.458	0.204	-0.275	-0.200	0.99	1.00	0.98
	$w_{w,opt}$	669	1128	1196	0.634	0.619	0.652	0.542	-0.271	-0.291	0.98	0.99	0.99
	$w_{w,opt}$ + 2%	570	877	690	0.803	0.707	0.827	0.177	-0.119	-0.178	0.99	1.00	1.00
AAS_50%	$w_{w,opt}$ - 2%	892	753	1686	0.692	0.594	0.568	0.213	0.716	-0.237	0.99	0.97	1.00
	$w_{w,opt}$	649	1289	1119	0.540	0.623	0.624	0.528	-0.277	-0.194	0.98	0.99	0.99
	$w_{w,opt}$ + 2%	557	1038	802	0.761	0.743	0.812	0.452	-0.273	-0.331	0.99	0.99	0.99
AAS_100%	$w_{w,opt}$ - 2%	2182	2381	3537	0.544	0.283	0.377	0.339	0.681	0.119	0.97	0.98	0.98
	$w_{w,opt}$	2787	2124	3330	0.234	0.205	0.371	0.353	0.694	0.093	0.98	0.95	0.99
	$w_{w,opt}$ + 2%	1418	2970	3275	0.487	0.233	0.303	0.184	0.200	0.160	0.94	0.98	0.99

Table 10. Fitting parameters (k_1, k_2, and k_3) of M-EPDG model from literature

Author	Materials	k_1	k_2	k_3
Farias et al. [75]	UCDW@30days (0-25 mm)	1302	0.01	1.25
Dong and Huang [76]	RA[1] (0-19 mm)	1450	0.98	-0.09
Hanifa et al. [77]	RC[2] (0-25 mm)	1008 ÷ 1263	0.82 ÷ 0.85	-0.22 ÷ -0.20
Hossain [73]	A-1-b[3] soil	954	0.46	-2.52
	A-2-4[3] soil	483 ÷ 1428	0.06 ÷ 0.65	-2.84 ÷ -0.88
Bassani et al. [13]	UCDW + 2% OPC[4] @ 28days (0-25 mm)	1117	1.66	-2.88
	UCDW + 10% CKD[5] @ 28days (0-25 mm)	1014	1.84	-3.44
MacDonald [78]	A-2-6[3] soil + 3% OPC[4] @ 28days (0-25 mm)	1465 ÷ 2953	0.47 ÷ 1.01	-0.11 ÷ 0.22
	A-2-4[3] soil + 3% OPC[4] @ 28days (0-25 mm)	2394 ÷ 2913	0.39 ÷ 0.77	-0.09 ÷ 0.57
Solanki et al. [79]	A-4[3] soil + 9% lime @ 28days	8462	0.01	-1.93
	A-4[3] soil + 10% FA[6] @ 28days	3705	0.02	-1.23
	A-4[3] soil + 10% CKD[5] @ 28days	3725	-0.02	-0.71

([1]) RA = Recycled Asphalt, ([2]) RC = Recycled Concrete, ([3]) according to AASHTO M 145 classification [80],
([4]) OPC = Ordinary Portland Cement, ([5]) CKD = Cement Kiln Dust, ([6]) FA = Fly Ash.

3.5 Field Emission Scanning Electron Microscopy (FESEM) and Energy Dispersive Spectroscopy (EDS) analyses

The microstructures of some alkali-activated samples are reported in Figure 11 and 12. In particular, Figure 11 shows the micrographs of samples prepared at $w_{w,opt}$, and activated with AAS_0% (A), AAS_50% (B) and AAS_100% (C), while in Figure 11D the sample with AAS_100% and $w_{w,opt}$ + 2% is depicted. Figure 12 provides higher magnification images of the samples in Figure11A and 11C.

The morphology profiles of samples prepared with AAS_0% and AAS_50% are quite similar, with clear evidence of the fact that primary UCDW particles are characterized by a wide range in size from a few to tens of microns, and that they form a poorly compact structure. Conversely, in the sample prepared with AAS_100%

there is almost no evidence of the original particles, while a compact and quite dense structure can be readily observed in contrast to the two previously mentioned materials.

Nevertheless, some cracks are present in this structure, as observed in geopolymers [81, 82, 83], which can be imputed to stresses arising in the produced glassy geopolymer phase during drying. The sample prepared with $w_{w,opt}$ + 2% presents a diffused residual porosity, attributable to the evaporation and draining phenomena brought about by an excess of water.

The higher magnification image of Figure 11A, reported in Figure 12A, provides clearer evidence of the presence of well-faceted uncoated particles, with no evidence of a binding layer between them. In contrast, the higher magnification image of the sample activated with AAS_100% (Figure 11C), reported in Figure 12B, shows an almost continuous rough coating and binding layer on the particle surface, attributable to the products of geopolymer reaction.

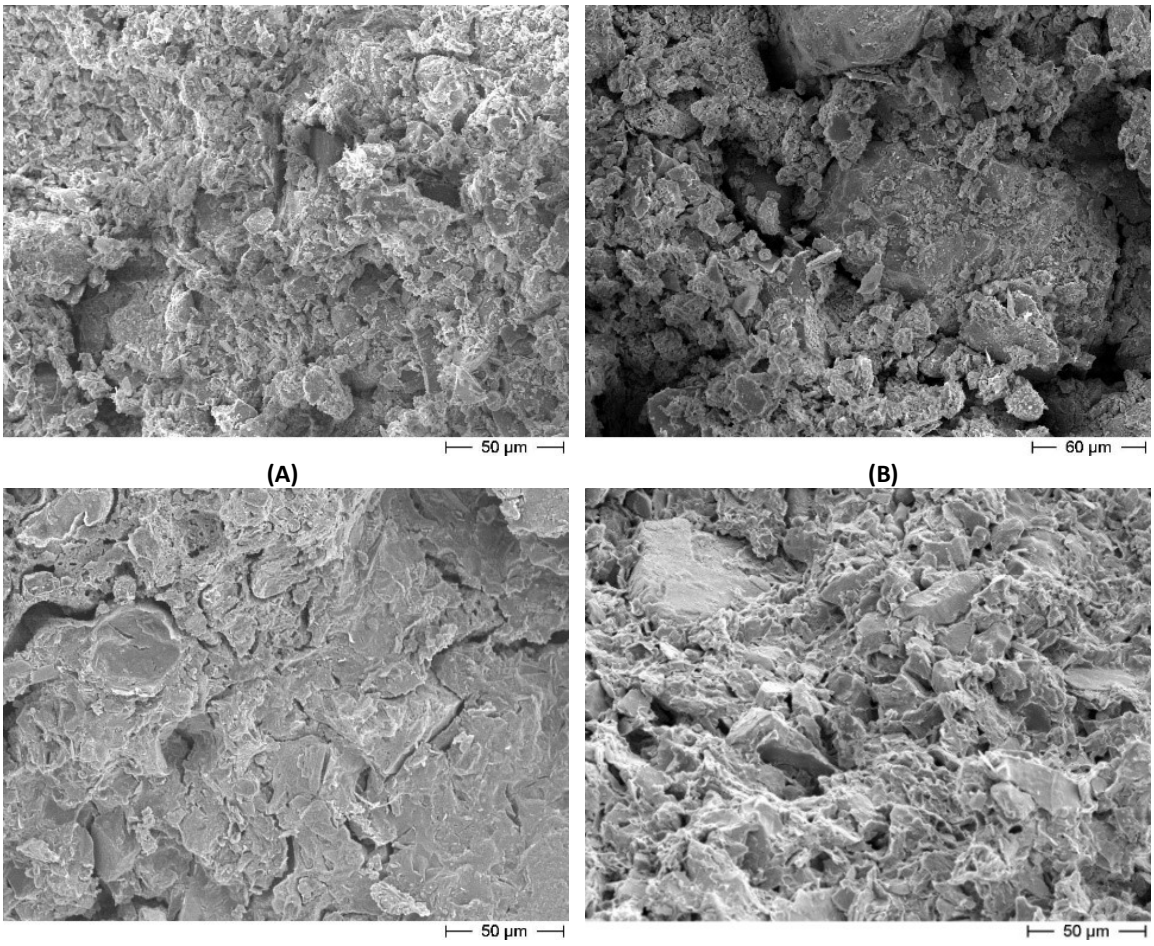

Figure 11. FESEM micrographs of samples prepared at $w_{w,opt}$, and activated with AAS_0% (A), AAS_50% (B) and AAS_100% (C). In (D) the sample with AAS_100% with $w_{w,opt}$ + 2%.

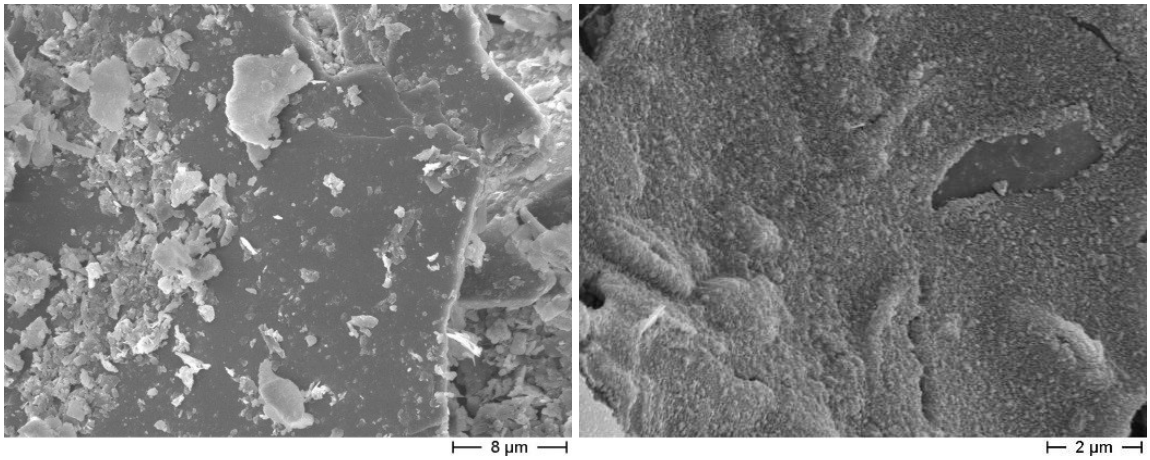

(A) **(B)**

Figure 12. FESEM micrographs of samples prepared at their optimal water content, and activated with AAS_0% (A) and AAS_100% (B), corresponding to samples in Figure 11A and Figure 11C respectively.

In order to confirm this hypothesis, several EDS analyses were carried out on both aggregates and surrounding layers. The results indicate a systematic Na enrichment in the binding layer when compared to close primary particles. Chemical analyses carried out on different coating areas showed that the Na/Si molar ratio always ranged between 0.8 and 1.5, a range that includes the nominal ratio of the activating solution (Na/Si molar ratio of 1.3). At the same time, in such a layer, *Ca* and *Al* elements were systematically detected. In different coating areas, the Al/Na molar ratio ranged between 0.17 and 0.28, while the Ca/Na molar ratio was between 0.19 and 0.25. These results suggest a preferential dissolution of *Ca* and *Al* ions from the UCDW particles, as induced by alkaline attack, and strengthen the hypothesis of a continuous sodium silicate-based coating, which could be reasonably attributed to the geopolymeric (partial) reaction between the activating solution and the UCDW fines.

However, the need for a greater insight into the geopolymer structure and a better understanding of the alkaline-activation phenomena in this complex system requires further investigation by means of other technologies, such as solid state nuclear magnetic resonance (SS-NMR) [84], and this work could be the subject of a future study. In addition, durability tests including water absorption, salt resistance, freeze-thaw cycling resistance and alkali silica reactions (ASR) will be carried out. As regards the ASR, the very high concentration of alkalis within these materials makes the alkali-silica reaction an actual degradation risk. On the other hand, the residual porosity of the material (Table 2), which is compatible with the envisaged application (i.e., stabilized granular materials to be used in subbase layers), renders any potential silica gel expansion due to ASR less harmful.

4. CONCLUSIONS

With the aim of reducing the use of Portland cement in road materials, the production of which is considered environmentally unfriendly, different by-products (*i.e.*, fly ash, cement kiln dust) have recently been put forward as alternative binders for the stabilization of recycled construction and demolition waste (CDW) aggregates. These by-products have also been alkali-activated in CDW mixtures rendering them suitable for use in the construction of pavement layers.

As an alternative to the addition of by-products rich in aluminosilicates, this investigation evaluated the use of a solution composed of sodium silicate and sodium hydroxide for the alkali activation of unselected construction and demolition waste (UCDW) aggregates. It is the presence of silica and aluminium in the fine particles which triggers the alkali activation process. Different AAS and UCDW aggregate mixtures were investigated in the laboratory using mechanical characterization (compressive and tensile strength, and resilient modulus), and through observation of the microscopic structure (FESEM analysis) and its chemical composition (EDS analysis).

The results documented here are promising, and offer a new perspective in the field of road constructions. The use of AAS-UCDW mixtures, which do not include natural aggregates and Portland cement, should be seen as an alternative and more sustainable option for the construction of subbase layers of new or rehabilitated road pavements.

The key findings of this research are as follows:

- the AAS solution made up of sodium silicate (29%) and sodium hydroxide (10%) in pure water (61%), indicated as AAS_100%, is able to trigger the alkali-activation of aluminosilicate compounds found in the finer grains of UCDW, and then significantly increase the strength and stiffness values of compacted recycled UCDW aggregates;
- at laboratory temperature (around 25°C), AAS_100% is more viscous and denser than water (which is always used to confer workability to unbound and stabilized granular materials in the laying phase); this has to be taken into account since both factors affect the compaction process of UCDW aggregates;
- excessive quantities of AAS in samples may lead to the saturation of permeable pores which can seriously compromise the effectiveness of the compacting effort, thus leaving a high residual void content in the solid matrix;
- with the reference grading curve and the UCDW aggregates investigated here, the best compaction results in terms of workability were found for an AAS content of around 10-11% in aggregate mass;
- compressive and tensile strength values of cured AAS-UCDW mixtures depend on the AAS concentration, on the quantity of AAS added to aggregates, and on the curing time; more specifically, the best UCS and ITS results were obtained for a content of 10% of AAS_100% in aggregate mass;

- after 7 days of curing, the ITS and UCS values of the AAS_100%-UCDW mixture satisfy the minimum requirements for cement stabilized granular mixtures for subbase layers of road pavements, and are within the typical range of results obtained with recycled and natural granular stabilized materials documented in literature; the same conclusions can be drawn for results obtained after 28 days of curing;
- a shear hardening behaviour at resilient modulus tests was observed for mixtures prepared with pure AAS for all the investigated curing times;
- an excessive quantity of AAS_100% in UCDW aggregates does not compromise the resilient properties of AAS stabilized UCDW aggregates after 60 days of curing;
- the use of diluted AAS (*i.e.*, made up of 50% of AAS and 50% of water) does not trigger the alkali-activation of UCDW fine particles; indirect tensile and compressive strength values were similar to those recorded for mixtures containing water only, and proved to be much lower than those for UCDW aggregates stabilized with AAS_100%;
- the FESEM and EDS analyses support the incidence of alkali-activation of fines included in UCDW recycled aggregates with AAS_100%.

This research has demonstrated that the alkali activation of UCDW aggregate fines is possible, and that it leads to a stabilized material with good mechanical performances. Compressive and tensile strength values are comparable to those in ordinary stabilized materials. The resilient response is comparable to those of typical materials suitable for use in base/subbase pavement layers. The use of this alternative material offers other important environmental and economic benefits. Regarding this last point, it should be noted that the current cost of UCDW aggregates is lower than that of natural ones for unbound pavement layers.

Notwithstanding the promising results documented here, future investigations are necessary to optimize the content and type of AAS, and to assess the environmental compatibility, durability, and resistance to permanent deformation of AAS-UCDW mixtures.

ACKNOWLEDGEMENTS

The authors greatly acknowledge CAVIT s.r.l. and INGESSIL S.r.l. for the provision of construction and demolition waste aggregates and sodium silicate respectively.

REFERENCES

[1] ISPRA, Rapporto Rifiuti Speciali, Istituto Superiore per la protezione e la ricerca ambientale, Rome, Italy, 2016.

[2] European Parliament, Directive 2008/98/EC of the European parliament and of the council of 19 November 2008 on waste and repealing certain directives (waste framework directive). 312(11-2b), 2008.

[3] J.R. Jiménez, J. Ayuso, A.P. Galvín, M. López, F. Agrela, Use of mixed recycled aggregates with a low embodied energy from non-selected CDW in unpaved rural roads, Constr. Build. Mater. 34 (2012) 34–43. doi:10.1016/j.conbuildmat.2012.02.042.
[4] J. de Brito, N. Saikia, Recycled Aggregate in Concrete, Springer London, London, 2013. http://link.springer.com/10.1007/978-1-4471-4540-0 (accessed October 27, 2016).
[5] T. Bennert, W. Papp Jr, A. Maher, N. Gucunski, Utilization of construction and demolition debris under traffic-type loading in base and subbase applications, Transp. Res. Rec. J. Transp. Res. Board. (2000) 33–39.
[6] A.R. Hill, A.R. Dawson, M. Mundy, Utilisation of aggregate materials in road construction and bulk fill, Resour. Conserv. Recycl. 32 (2001) 305–320. doi:10.1016/S0921-3449(01)00067-2.
[7] C.S. Poon, D. Chan, Feasible use of recycled concrete aggregates and crushed clay brick as unbound road sub-base, Constr. Build. Mater. 20 (2006) 578–585. doi:10.1016/j.conbuildmat.2005.01.045.
[8] A. Arulrajah, J. Piratheepan, M.M. Disfani, M.W. Bo, Resilient Moduli Response of Recycled Construction and Demolition Materials in Pavement Subbase Applications, J. Mater. Civ. Eng. 25 (2013) 1920–1928. doi:10.1061/(ASCE)MT.1943-5533.0000766.
[9] D.X. Xuan, A.A.A. Molenaar, L.J.M. Houben, Evaluation of cement treatment of reclaimed construction and demolition waste as road bases, J. Clean. Prod. 100 (2015) 77–83. doi:10.1016/j.jclepro.2015.03.033.
[10] I. Del Rey, J. Ayuso, A. Barbudo, A.P. Galvín, F. Agrela, J. de Brito, Feasibility study of cement-treated 0–8 mm recycled aggregates from construction and demolition waste as road base layer, Road Mater. Pavement Des. 17 (2016) 678–692. doi:10.1080/14680629.2015.1108221.
[11] Y. Hou, X. Ji, L. Zou, S. Liu, X. Su, Performance of cement-stabilised crushed brick aggregates in asphalt pavement base and subbase applications, Road Mater. Pavement Des. 17 (2016) 120–135. doi:10.1080/14680629.2015.1064466.
[12] A. Arulrajah, A. Mohammadinia, A. D'Amico, S. Horpibulsuk, Cement kiln dust and fly ash blends as an alternative binder for the stabilization of demolition aggregates, Constr. Build. Mater. 145 (2017) 218–225. doi:10.1016/j.conbuildmat.2017.04.007.
[13] M. Bassani, P.P. Riviera, L. Tefa, Short-Term and Long-Term Effects of Cement Kiln Dust Stabilization of Construction and Demolition Waste, J. Mater. Civ. Eng. 29 (2016) 04016286. doi:10.1061/(ASCE)MT.1943-5533.0001797.
[14] C. Shi, D. Roy, P. Krivenko, Alkali-Activated Cements and Concretes, CRC Press, 2006.
[15] J.L. Provis, Geopolymers and other alkali activated materials: why, how, and what?, Mater. Struct. 47 (2014) 11–25. doi:10.1617/s11527-013-0211-5.
[16] D.N. Huntzinger, T.D. Eatmon, A life-cycle assessment of Portland cement manufacturing: comparing the traditional process with alternative technologies, J. Clean. Prod. 17 (2009) 668–675. doi:10.1016/j.jclepro.2008.04.007.
[17] E. Worrell, L. Price, N. Martin, C. Hendriks, L.O. Meida, Carbon dioxide emissions from the global cement industry, Annu. Rev. Energy Environ. 26 (2001) 303–329.
[18] C. Li, X.Z. Gong, S.P. Cui, Z.H. Wang, Y. Zheng, B.C. Chi, CO_2 Emissions due to Cement Manufacture, Mater. Sci. Forum. 685 (2011) 181–187. doi:10.4028/www.scientific.net/MSF.685.181.
[19] J.X. Peng, L. Huang, Y.B. Zhao, P. Chen, L. Zeng, W. zheng, Modeling of Carbon Dioxide Measurement on Cement Plants, Adv. Mater. Res. 610–613 (2012) 2120–2128. doi:10.4028/www.scientific.net/AMR.610-613.2120.
[20] P. Duxson, J.L. Provis, G.C. Lukey, J.S.J. van Deventer, The role of inorganic polymer technology in the development of 'green concrete,' Cem. Concr. Res. 37 (2007) 1590–1597. doi:10.1016/j.cemconres.2007.08.018.
[21] J.S.J. van Deventer, J.L. Provis, P. Duxson, D.G. Brice, Chemical Research and Climate Change as Drivers in the Commercial Adoption of Alkali Activated Materials, Waste Biomass Valorization. 1 (2010) 145–155. doi:10.1007/s12649-010-9015-9.
[22] G. Habert, J.B. d'Espinose de Lacaillerie, N. Roussel, An environmental evaluation of geopolymer based concrete production: reviewing current research trends, J. Clean. Prod. 19 (2011) 1229–1238. doi:10.1016/j.jclepro.2011.03.012.

[23] B.C. McLellan, R.P. Williams, J. Lay, A. van Riessen, G.D. Corder, Costs and carbon emissions for geopolymer pastes in comparison to ordinary portland cement, J. Clean. Prod. 19 (2011) 1080–1090. doi:10.1016/j.jclepro.2011.02.010.
[24] L.K. Turner, F.G. Collins, Carbon dioxide equivalent (CO2-e) emissions: A comparison between geopolymer and OPC cement concrete, Constr. Build. Mater. 43 (2013) 125–130. doi:10.1016/j.conbuildmat.2013.01.023.
[25] C.H. Hurley, T.H. Thornburn, Sodium silicate stabilization of soils: A review of the literature, Soil Mechanics Laboratory, Department of Civil Engineering, Engineering Experiment Station, University of Illinois, 1971.
[26] A. Allahverdi, E.N. Kani, Construction wastes as raw materials for geopolymer binders, Int J Civ. Eng. 7 (2009) 154–160.
[27] S. Ahmari, X. Ren, V. Toufigh, L. Zhang, Production of geopolymeric binder from blended waste concrete powder and fly ash, Constr. Build. Mater. 35 (2012) 718–729. doi:10.1016/j.conbuildmat.2012.04.044.
[28] A. Pathak, S. Kumar, V.K. Jha, Development of Building Material from Geopolymerization of Construction and Demolition Waste (CDW), Trans. Indian Ceram. Soc. 73 (2014) 133–137. doi:10.1080/0371750X.2014.922429.
[29] K. Komnitsas, D. Zaharaki, A. Vlachou, G. Bartzas, M. Galetakis, Effect of synthesis parameters on the quality of construction and demolition wastes (CDW) geopolymers, Adv. Powder Technol. 26 (2015) 368–376. doi:10.1016/j.apt.2014.11.012.
[30] S.R. Zedan, M.R. Mohamed, D.A. Ahmed, A.H. Mohammed, Effect of demolition/construction wastes on the properties of alkali activated slag cement, HBRC J. (2015). doi:10.1016/j.hbrcj.2015.12.001.
[31] V.K. Jha, A. Tuladhar, An attempt of geopolymer synthesis from construction waste, J. Nepal Chem. Soc. 28 (2013) 29–33.
[32] European Committee for Standardization, Tests for mechanical and physical properties of aggregates - Part 6: Determination of particle density and water absorption, 2013.
[33] Centro Interuniversitario Sperimentale di Ricerca Stradale, Norme Tecniche Prestazionali per Capitolati Speciali d'Appalto, 2001.
[34] L.N. Assi, E. Eddie Deaver, P. Ziehl, Effect of source and particle size distribution on the mechanical and microstructural properties of fly Ash-Based geopolymer concrete, Constr. Build. Mater. 167 (2018) 372–380. doi:10.1016/j.conbuildmat.2018.01.193.
[35] K.-H. Yang, J.-K. Song, Workability Loss and Compressive Strength Development of Cementless Mortars Activated by Combination of Sodium Silicate and Sodium Hydroxide, J. Mater. Civ. Eng. 21 (2009) 119–127. doi:10.1061/(ASCE)0899-1561(2009)21:3(119).
[36] Antoni, D. Wiyono, A. Vianthi, P. Putra, G. Kartadinata, D. Hardjito, Effect of Particle Size on Properties of Sidoarjo Mud-Based Geopolymer, Mater. Sci. Forum. 803 (2014) 44–48. doi:10.4028/www.scientific.net/MSF.803.44.
[37] F. Mádai, F. Kristály, G. Mucsi, Microstructure, mineralogy and physical properties of ground fly ash based geopolymers, Ceram-Silikáty. 59 (2015) 70–79.
[38] F. Agrela, M. Sánchez de Juan, J. Ayuso, V.L. Geraldes, J.R. Jiménez, Limiting properties in the characterisation of mixed recycled aggregates for use in the manufacture of concrete, Constr. Build. Mater. 25 (2011) 3950–3955. doi:10.1016/j.conbuildmat.2011.04.027.
[39] G. Cerni, S. Colagrande, Resilient Modulus of Recycled Aggregates Obtained by Means of Dynamic Tests in a Triaxial Apparatus, Procedia - Soc. Behav. Sci. 53 (2012) 475–484. doi:10.1016/j.sbspro.2012.09.898.
[40] Z. Sun, H. Cui, H. An, D. Tao, Y. Xu, J. Zhai, Q. Li, Synthesis and thermal behavior of geopolymer-type material from waste ceramic, Constr. Build. Mater. 49 (2013) 281–287. doi:10.1016/j.conbuildmat.2013.08.063.
[41] D. Zaharaki, M. Galetakis, K. Komnitsas, Valorization of construction and demolition (C&D) and industrial wastes through alkali activation, Constr. Build. Mater. 121 (2016) 686–693. doi:10.1016/j.conbuildmat.2016.06.051.
[42] N. Cristelo, P. Tavares, E. Lucas, T. Miranda, D. Oliveira, Quantitative and qualitative assessment of the amorphous phase of a Class F fly ash dissolved during alkali activation reactions – Effect of mechanical

activation, solution concentration and temperature, Compos. Part B Eng. 103 (2016) 1–14. doi:10.1016/j.compositesb.2016.08.001.
[43] L.N. Tchadjie, S.O. Ekolu, Enhancing the reactivity of aluminosilicate materials toward geopolymer synthesis, J. Mater. Sci. 53 (2018) 4709–4733. doi:10.1007/s10853-017-1907-7.
[44] P. Palmero, A. Formia, J.-M. Tulliani, P. Antonaci, Valorisation of alumino-silicate stone muds: From wastes to source materials for innovative alkali-activated materials, Cem. Concr. Compos. 83 (2017) 251–262. doi:10.1016/j.cemconcomp.2017.07.011.
[45] H. Tchakoute Kouamo, J.A. Mbey, A. Elimbi, B.B. Kenne Diffo, D. Njopwouo, Synthesis of volcanic ash-based geopolymer mortars by fusion method: Effects of adding metakaolin to fused volcanic ash, Ceram. Int. 39 (2013) 1613–1621. doi:10.1016/j.ceramint.2012.08.003.
[46] X. Yang, W. Zhu, Q. Yang, The Viscosity Properties of Sodium Silicate Solutions, J. Solut. Chem. 37 (2008) 73–83. doi:10.1007/s10953-007-9214-6.
[47] European Committee for Standardization, Unbound and hydraulically bound mixtures - Part 2: Test methods for laboratory reference density and water content - Proctor compaction, 2010.
[48] M. Bassani, L. Tefa, Compaction and freeze-thaw degradation assessment of recycled aggregates from unseparated construction and demolition waste, Constr. Build. Mater. 160 (2018) 180–195. doi:10.1016/j.conbuildmat.2017.11.052.
[49] American Association of State and Highway Transportation Officials, Standard method of test for determining the resilient modulus of soils and aggregate materials, 2013.
[50] G. Cerni, S. Camilli, Comparative Analysis of Gyratory and Proctor Compaction Processes of Unbound Granular Materials, Road Mater. Pavement Des. 12 (2011) 397–421. doi:10.3166/rmpd.12.397-421.
[51] N. Cristelo, A. Fernández-Jiménez, C. Vieira, T. Miranda, Á. Palomo, Stabilisation of construction and demolition waste with a high fines content using alkali activated fly ash, Constr. Build. Mater. 170 (2018) 26–39. doi:10.1016/j.conbuildmat.2018.03.057.
[52] K. Parthiban, K. Saravana Raja Mohan, Effect of Sodium Hydroxide Concentration and Alkaline Ratio on the Compressive Strength of Slag Based Geopolymer Concrete, Int. J. ChemTech Res. 6 (2014) 974–4290.
[53] A.B. Malkawi, M.F. Nuruddin, A. Fauzi, H. Almattarneh, B.S. Mohammed, Effects of Alkaline Solution on Properties of the HCFA Geopolymer Mortars, Procedia Eng. 148 (2016) 710–717. doi:10.1016/j.proeng.2016.06.581.
[54] J. Davidovits, Geopolymer Chemistry and Applications, Third edition, Geopolymer Institute, Saint-Quentin, 2011.
[55] T.T. Kien, L.T. Thanh, P.V. Lu, Utilisation of construction demolition waste as stabilised materials for road base applications, in: Int. Conf. Sustain. Built Environ. Future Hanoi, 2013: p. 27.
[56] A. Mohammadinia, A. Arulrajah, J. Sanjayan, M.M. Disfani, M.W. Bo, S. Darmawan, Laboratory Evaluation of the Use of Cement-Treated Construction and Demolition Materials in Pavement Base and Subbase Applications, J. Mater. Civ. Eng. 27 (2014) 04014186. doi:10.1061/(ASCE)MT.1943-5533.0001148.
[57] D.R. Biswal, U.C. Sahoo, S.R. Dash, Strength and Stiffness Studies of Cement Stabilized Granular Lateritic Soil, in: W. Frikha, S. Varaksin, A. Viana da Fonseca (Eds.), Soil Test. Soil Stab. Ground Improv., Springer International Publishing, Cham, 2018: pp. 320–336. doi:10.1007/978-3-319-61902-6_25.
[58] S. Lim, D. Zollinger, Estimation of the compressive strength and modulus of elasticity of cement-treated aggregate base materials, Transp. Res. Rec. J. Transp. Res. Board. (2003) 30–38.
[59] J. Piratheepan, C.T. Gnanendran, S.-C. Lo, Characterization of cementitiously stabilized granular materials for pavement design using unconfined compression and IDT testings with internal displacement measurements, J. Mater. Civ. Eng. 22 (2009) 495–505.
[60] K.A. Davis, L.S. Warr, S.E. Burns, E.J. Hoppe, Physical and Chemical Behavior of Four Cement-Treated Aggregates, J. Mater. Civ. Eng. 19 (2007) 891–897. doi:10.1061/(ASCE)0899-1561(2007)19:10(891).
[61] American Society for Testing Materials, Standard Practice for Classification of Soils for Engineering Purposes (Unified Soil Classification System), 2011.
[62] D.R.M. Brew, K.J.D. MacKenzie, Geopolymer synthesis using silica fume and sodium aluminate, J. Mater. Sci. 42 (2007) 3990–3993. doi:10.1007/s10853-006-0376-1.

[63] C. Marín-López, J.L. Reyes Araiza, A. Manzano-Ramírez, J.C. Rubio Avalos, J.J. Perez-Bueno, M.S. Muñiz-Villareal, E. Ventura-Ramos, Y. Vorobiev, Synthesis and characterization of a concrete based on metakaolin geopolymer, Inorg. Mater. 45 (2009) 1429–1432. doi:10.1134/S0020168509120231.
[64] U. Rattanasak, P. Chindaprasirt, Influence of NaOH solution on the synthesis of fly ash geopolymer, Miner. Eng. 22 (2009) 1073–1078. doi:10.1016/j.mineng.2009.03.022.
[65] K. Somna, C. Jaturapitakkul, P. Kajitvichyanukul, P. Chindaprasirt, NaOH-activated ground fly ash geopolymer cured at ambient temperature, Fuel. 90 (2011) 2118–2124. doi:10.1016/j.fuel.2011.01.018.
[66] P. Duxson, J.L. Provis, G.C. Lukey, S.W. Mallicoat, W.M. Kriven, J.S.J. van Deventer, Understanding the relationship between geopolymer composition, microstructure and mechanical properties, Colloids Surf. Physicochem. Eng. Asp. 269 (2005) 47–58. doi:10.1016/j.colsurfa.2005.06.060.
[67] F. Pacheco-Torgal, J. Castro-Gomes, S. Jalali, Alkali-activated binders: A review. Part 1. Historical background, terminology, reaction mechanisms and hydration products, Constr. Build. Mater. 22 (2008) 1305–1314. doi:10.1016/j.conbuildmat.2007.10.015.
[68] A. Allahverdi, E.N. Kani, Use of construction and demolition waste (CDW) for alkali-activated or geopolymer cements, in: Handb. Recycl. Concr. Demolition Waste, Elsevier, 2013: pp. 439–475.
[69] A. Naghizadeh, S.O. Ekolu, Pozzolanic materials and waste products for formulation of geopolymer cements in developing countries: a review, (2017).
[70] American Association of State Highway and Transportation Officials, Mechanistic-empirical pavement design guide: a manual of practice., 2015.
[71] M.D. Nazzal, L.N. Mohammad, Estimation of resilient modulus of subgrade soils for design of pavement structures, J. Mater. Civ. Eng. 22 (2010) 726–734.
[72] H.H. Titi, M.B. Elias, S. Helwany, Determination of Typical Resilient Modulus Values for Selected Soils in Wisconsin, Wisconsin Department of Transportation Division of Transportation Infrastructure Development Research Coordination Section, Milwaukee, WI, 2006.
[73] M. Hossain, Estimation of Subgrade Resilient Modulus for Virginia Soil, Transp. Res. Rec. J. Transp. Res. Board. 2101 (2009) 98–109. doi:10.3141/2101-12.
[74] A. Yau, H.L. Von Quintus, Study of LTPP Laboratory Resilient Modulus Test Data and Response Characteristics, Federal Highway Administration Office of Infrastructure Research and Development Federal Highway Administration, Georgetown Pike McLean, VA, 2002.
[75] M. Farias, A. Gomez, F. Quiñones Sinisterra, Use of recycled aggregates from construction and demolition wastes for the construction of flexible pavements, in: Third Int. Conf. Geotech. Constr. Mater. Environ., Nagoya, Japan, 2013.
[76] Q. Dong, B. Huang, Laboratory evaluation on resilient modulus and rate dependencies of RAP used as unbound base material, J. Mater. Civ. Eng. 26 (2013) 379–383.
[77] K. Hanifa, M.Y. Abu-Farsakh, G. Gavin, Design Values of Resilient Modulus for Stabilized and Non-Stabilized Base, Louisiana Department of Transportation and Development, Baton Rouge, LA, 2015.
[78] W.M. MacDonald, Resilient Modulus and Strength Index Properties of Stabilized Base for Tennessee Highways, University of Tennessee, 2008.
[79] P. Solanki, M. Zaman, J. Dean, Resilient Modulus of Clay Subgrades Stabilized with Lime, Class C Fly Ash, and Cement Kiln Dust for Pavement Design, Transp. Res. Rec. J. Transp. Res. Board. 2186 (2010) 101–110. doi:10.3141/2186-11.
[80] American Association of State and Highway Transportation Officials, Specification for Classification of Soils and Soil-Aggregate Mixtures for Highway Construction Purposes, 2012.
[81] M. Catauro, F. Papale, G. Lamanna, F. Bollino, Geopolymer/PEG Hybrid Materials Synthesis and Investigation of the Polymer Influence on Microstructure and Mechanical Behavior, Mater. Res. 18 (2015) 698–705. doi:10.1590/1516-1439.342814.
[82] P. Timakul, W. Rattanaprasit, P. Aungkavattana, Improving compressive strength of fly ash-based geopolymer composites by basalt fibers addition, Ceram. Int. 42 (2016) 6288–6295. doi:10.1016/j.ceramint.2016.01.014.
[83] F. Matalkah, P. Soroushian, A. Balchandra, A. Peyvandi, Characterization of Alkali-Activated Nonwood Biomass Ash–Based Geopolymer Concrete, J. Mater. Civ. Eng. 29 (2017) 04016270.

[84] Y.-L. Tsai, J.V. Hanna, Y.-L. Lee, M.E. Smith, J.C.C. Chan, Solid-state NMR study of geopolymer prepared by sol–gel chemistry, J. Solid State Chem. 183 (2010) 3017–3022. doi:10.1016/j.jssc.2010.10.008.